

Taxonomy and toxicity of a bloom-forming *Ostreopsis* species (Dinophyceae, Gonyaulacales) in Tahiti island (South Pacific Ocean): one step further towards resolving the identity of *O. siamensis*.

Chomérat Nicolas ^{1,*}, Bilién Gwenaél ¹, Viallon Jérôme ², Hervé Fabienne ³, Réveillon Damien ³, Henry Kévin ², Zubia Mayalen ⁴, Vieira Christophe ⁵, Ung André ², Gatti Clémence Mahana Iti ², Roué Mélanie ², Derrien Amélie ^{1,6}, Amzil Zouher ³, Darius Hélène Taiana ², Chinain Mireille ²

¹ Ifremer, LER BO, Station of Marine Biology of Concarneau, Place de la Croix, F-29900 Concarneau, France

² Institut Louis Malardé, Laboratoire des Micro-algues toxiques, UMR 241-EIO, PO box 30, 98713 Papeete, Tahiti, French Polynesia

³ Ifremer, Phycotoxins Laboratory, BP 21105, F-44311 Nantes Cedex 3, France

⁴ Université de Polynésie Française, UMR 241-EIO, PO Box 6570, 98702 Faa'a, Tahiti, French Polynesia

⁵ Kobe University Research Center for Inland Seas, Rokkodai, Kobe 657-8501, Japan

⁶ Institut de Recherche pour le Développement (IRD), UMR 241-EIO, PO box 529, 98713 Papeete, Tahiti, French Polynesia

* Corresponding author : Nicolas Chomérat, email address : nicolas.chomerat@ifremer.fr

Abstract :

Among dinoflagellates responsible for benthic harmful algal blooms, the genus *Ostreopsis* primarily described from tropical areas has been increasingly reported from subtropical and temperate areas worldwide. Several species of this toxigenic genus produce analogs of palytoxin, thus representing a major threat to human and environmental health. The taxonomy of several species needs to be clarified as it was based mostly on morphological descriptions leading in some cases to ambiguous interpretations and misidentifications. The present study aims at reporting a benthic bloom that occurred in April 2019 in Tahiti island, French Polynesia. A complete taxonomic investigation of the blooming *Ostreopsis* species was realized using light, epifluorescence and field emission electron microscopy and phylogenetic analyses inferred from LSU rDNA and ITS–5.8S rDNA regions. Toxicity of a natural sample and strains isolated from the bloom was assessed using both neuroblastoma cell-based assay and LC-MS/MS analyses. Morphological observations showed that cells were round to oval, large, 58.0–82.5 µm deep (dorso-ventral length) and 45.7–61.2 µm wide. The cingulum was conspicuously undulated, forming a ‘V’ in ventral view. Thecal plates possessed large pores in depressions, with a collar rim. Detailed observation also revealed the presence of small thecal pores invisible in LM. Phylogenetic analyses were congruent and all sequences clustered within the genotype *Ostreopsis* sp. 6, in a subclade closely related to sequences from the Gulf of Thailand and Malaysia. No toxicity was found on the field sample but all the strains isolated from the bloom were found to be cytotoxic and produced ostreocin D, a lower amount of ostreocins A and B and putatively other compounds. Phylogenetic data demonstrate the presence of this

species in the Gulf of Thailand, at the type locality of *O. siamensis*, and morphological data are congruent with the original description and support this identification.

Highlights

► A benthic *Ostreopsis* bloom is described from tahiti Island, french polyensia. ► Taxonomy and toxicity are analyzed from a bloom sample and 8 isolated strains. ► The specimens belong to *Ostreopsis* sp. 6 and are morphologically close to *O. siamensis*. ► Phylogenetic data reveal a close relationship with strains from the gulf of Thailand. ► All the 8 strains studied are cytotoxic using CBA-N2a, and produce mostly OST-D.

Keywords : Dinoflagellate, ITS–5.8S rDNA, LSU rDNA, Microscopy, Morphology, Ostreocin, Phylogeny

1. Introduction

Tropical regions are endemically affected by outbreaks of ciguatera fish poisoning (CFP) linked to the proliferation of the toxic dinoflagellate genus *Gambierdiscus* R.Adachi & Y.Fukuyo (Berdalet et al., 2017; Chinain et al., 2020). Other benthic dinoflagellate genera, such as *Ostreopsis* Johs. Schmidt, *Prorocentrum* Ehrenberg and *Coolia* Meunier, have been shown to regularly co-occur with *Gambierdiscus* in epiphytic/benthic assemblages in tropical areas (*e.g.*, Besada et al., 1982; Chinain et al., 2016; Smith et al., 2017). The genus *Ostreopsis* was originally described from plankton samples from the Gulf of Thailand (Schmidt, 1901), but it received little attention for about 80 years. It gained a new interest when Fukuyo (1981) conducted a survey of benthic dinoflagellates potentially responsible for CFP in islands of the Pacific region. Since this date, the number of described *Ostreopsis* species has continued to increase, with frequent occurrence reports from tropical ciguateric areas (Bagnis et al., 1985; Carlson and Tindall, 1985; Ballantine et al., 1988).

Although the first report of an *Ostreopsis* bloom in the Mediterranean by F.J.R. Taylor can be dated back to 1972 (GEOHAB, 2012), since the 90s, blooms have become more frequently mentioned along the Mediterranean Sea, Atlantic, New Zealand, Japanese, Russian and Australian coasts (*e.g.*, Tognetto et al., 1995; Vila et al., 2001; Mangialajo et al., 2008; Shears and Ross, 2009; Selina and Orlova, 2010; Coahu et al., 2011; Sato et al., 2011; Parsons et al., 2012; David et al., 2013; Accoroni and Totti, 2016; Verma et al., 2020). The apparent expansion of *Ostreopsis* for the past 30 years is mainly attributable to the species *O. cf. ovata* and *O. cf. siamensis* in temperate (Accoroni and Totti, 2016) and subtropical areas (Nascimento et al., 2012; Tibiriçá et al., 2019; Verma et al., 2020). *Ostreopsis* blooms have been consistently described as forming an apparent brownish mucilaginous and filamentous matrix covering macroalgae or substratum, sometimes

extending over large areas, and which can detach and float freely (Vila et al., 2001; Shears and Ross, 2009; GEOHAB, 2012; Tibiriçá et al., 2019).

The massive blooms of the genus *Ostreopsis* cause threats to human health in certain urbanized, temperate areas and are responsible for health concerns and beach closures (Tester et al., 2020). Respiratory illness and skin irritation have been associated with *Ostreopsis* blooms in the Mediterranean and its adjacent seas (e.g., Tichadou et al., 2010; GEOHAB, 2012; Berdalet et al., 2017). These effects have been attributed to analogues of palytoxin (PITX), a highly toxic and water soluble molecule originally described from the zoanthid *Palythoa toxica* (Moore and Scheuer, 1971). A considerable number of analogs have been identified in *Ostreopsis* spp., such as ostreocins (OSTs) (Usami et al., 1995; Terajima et al., 2018a) and ovatoxins (OvTXs) (Ciminiello et al., 2008; Tartaglione et al., 2017). However, the effects of these molecules on human health still need to be investigated more deeply (Tester et al., 2020). Indeed, OvTXs were detected in aerosols (Ciminiello et al., 2014) and can also be bio-accumulated in marine organisms (Amzil et al., 2012; Brissard et al., 2014). In tropical areas, fatalities have been attributed to PITX-like molecules, and it has been suggested that *Ostreopsis* spp. are involved in a particular type of poisoning called clupeotoxism (Alcala et al., 1988; Onuma et al., 1999) which is still controversial (Randall, 2005). Besides effects to humans, blooms have caused mortality among benthic invertebrates such as sea urchins in Brazil (Ferreira, 2006) and New Zealand (Shears and Ross, 2009). Moreover, a negative impact of *Ostreopsis* spp. has been shown on several benthic organisms (Guidi-Guilvard et al., 2012; Neves et al., 2018; Pavaux et al., 2019), which may lead to modifications of benthic communities in the concerned areas.

Toxicity of *Ostreopsis* species has been shown to vary within and among species, from non toxic to producing up to 468 pg [total OvTXs] per cell (e.g., Nascimento et al., 2012; Tartaglione et al., 2017). In addition to natural variability, some contradictory reports of their toxicity and toxin content are likely due to the existence of cryptic species or possible misidentifications (Tester et al.,

2020). Studies aiming at collecting physiological and toxicological data from genetically identified isolates of *Ostreopsis* species are critically needed (Tester et al., 2020). As emphasized by many authors (Rhodes, 2011; Parsons et al., 2012; Hoppenrath et al., 2014; Tester et al., 2020), the taxonomy of *Ostreopsis* genus is problematic and requires a major revision. One of the challenges is to reconcile traditional taxonomy based on morphological features and molecular taxonomy that has allowed to unveil several genotypes not yet fully characterized (Sato et al., 2011; Chomérat et al., 2019). Hence, resolving the issues of *Ostreopsis* taxonomy is fundamental for efficient monitoring of their distribution trends and to interpret environmental influences on their population dynamics in a context of climate change (Berdalet et al., 2017; Tester et al., 2020).

The diversity of *Ostreopsis* has been only poorly studied in the islands from the mid-Pacific, including French Polynesia since it was not considered problematic contrary to *Gambierdiscus*. To date, only two species have been reported, namely *O. ovata* Y.Fukuyo and *O. lenticularis* Y.Fukuyo (Fukuyo, 1981). Bagnis et al. (1985) investigated the population dynamics of three benthic dinoflagellates in French Polynesia and suggested that *O. lenticularis* became the major component of the reef dinoflagellate community following *Gambierdiscus* bloom. Moreover, in contrast with *Gambierdiscus*, *O. lenticularis* was suspected not to be toxic (Bagnis et al., 1985), which has been fully confirmed recently (Chomérat et al., 2019). Except for the first observations by Fukuyo (1981) in French Polynesia and New Caledonia, no additional data concerning *O. ovata* have been reported from French Polynesia and this species definitely deserves more thorough investigations. More recently, Rhodes et al. (2017) identified another genotype, *Ostreopsis* sp. 3, in the poorly studied Kermadec Islands (a New Zealand territory), 1000 km northeast of New Zealand, but genetic data also showed its presence in the Cook Islands which are closer to French Polynesia. By contrast, in the western Pacific, Sato et al. (2011) made a remarkable study and identified a wider diversity, including several undescribed genotypes that still need to be assigned taxonomically.

In April 2019, a very unusual benthic bloom was detected during a field survey conducted on the western coast of Tahiti Island. Preliminary observations revealed it was dominated almost exclusively by *Ostreopsis* cells, although some pennate diatoms were also visible. The present study provides a taxonomic identification of the *Ostreopsis* species responsible for the bloom and describes its toxic potential. To this end, scanning electron microscopy (SEM) observations combined with phylogenetic analyses were performed on field samples. In addition, the toxic status of the wild bloom sample and monoclonal cultures further established from this bloom was assessed using the mouse neuroblastoma cell-based assay (CBA-N2a) in parallel with liquid chromatography coupled with tandem mass spectrometry (LC-MS/MS) to identify the toxic compounds, if any.

2. Material and methods

2.1 Sampling area and description of the wild bloom

The benthic bloom described in this study occurred at Toaroto Beach (17.64046°S; 149.610259°W) in the municipality of Punaauia, Tahiti Island (Fig. 1). It was discovered on April 2019, at the end of the rainy season, on the reef located *ca.* 20 m off the Toaroto Beach. It covered the entire reef over a radial of *ca.* 30 m between the shore and the barrier reef, and presented as a thin, filamentous and mucilaginous brownish mat covering abiotic (*e.g.*, bedrock) and biotic substrates including macroalgae (*e.g.*, *Turbinaria ornata*, *Dictyota bartayresiana*), sponges and corals (*e.g.*, *Porites*, *Pocillopora*) (Fig. 2A–C).

The bloom was sampled between 0-2 m depth using two classical methods: cells found floating on the surface attached to mucus threads were skimmed using a dip net (100 µm porosity) positioned facing the current. Epiphytic cells of *Ostreopsis* were dislodged and collected from *T. ornata* by gently shaking macroalgal samples nearby a dip net. The sea water temperature at the time of sampling was 27 °C. Both samples were then pooled and transferred into a 1 L double-cap

container. Three sub-samples were taken for further *in vitro* culturing assays, SEM observations (preserved in 2.5% glutaraldehyde) and DNA amplification and sequencing (preserved in Lugol's solution), respectively. The remaining bloom sample was freeze-dried for 20 h at -20°C, 1 mbar, then 4 h at -60°C, 0.01 mbar (Martin Christ, Beta 1-8 LDplus). The resulting dry sample was weighted (11 g) and stored at 4°C until further extraction.

2.2 *In vitro* culturing of *Ostreopsis*

Ostreopsis clonal cultures were established from single cells isolated from field samples of the bloom, using an inverted microscope. They were routinely maintained in Fernbach flasks seeded with 100 mL of cell inoculum and 1 L of f10k enriched natural seawater (NSW) culture medium (Holmes et al., 1991), at 26 ± 1 °C, a salinity of 36, under 60 ± 10 $\mu\text{mol photons m}^{-2}\text{s}^{-1}$ irradiance, in a 12 h light:12 h dark photoperiod. After a growth period of ≈ 35 days, cells were harvested at their stationary growth phase by filtration and centrifugation. Cell counts were achieved using a Coulter counter (Beckman) and the resulting cell pellets freeze-dried and weighted for toxicity and toxin analyses.

Eight strains were analyzed in the present study (PNA19-1 to -4 and PNA19-6 to -9). These strains are part of the algal collection of the Laboratory of Marine Biotoxins of the Institut Louis Malardé (Tahiti, French Polynesia), where cultures are deposited. All the following experiments were conducted on non-axenic acclimated batch cultures.

2.3 *Microscopy observations*

Light microscopy (LM) observations were conducted on live cells of 5-10 days of age using a Leica DMLB microscope (Leica, Wetzlar, Germany) equipped with a D850 DSLR camera (Nikon, Tokyo, Japan). Epifluorescence images were realized with a Universal microscope (Zeiss,

Oberkochen, Germany) after staining cells with Solophenyl Flavine 7GFE500. A small drop of the stock solution (0.1% w/v) was added to a drop of water containing isolated cells fixed in Lugol's solution. Epifluorescence observations were carried out using a FITC (blue excitation/green emission) filter set (Chomérat et al., 2017).

Cells isolated from the bloom were observed using field-emission SEM (FE-SEM). Prior to scanning electron microscopy, cells fixed in 2.5% glutaraldehyde from the field sample were first isolated using a micropipette, rinsed several times in distilled water and processed according to Chomérat and Couté (2008). Briefly, cells were trapped between two polycarbonate membranes (Isopore RTTP, pores 1.2 μm , Merck Millipore, Molsheim, France) attached with a paper clamp, so they can be processed with minimum losses. Dehydration was carried out in ethanol baths of 15%, 30%, 50%, 70%, 95% vol. ethanol (about 20 min in each bath), and several baths of absolute ethanol (100%) and then cells were critical point dried using an EMS 850 (Electron Microscopy Sciences, Hatfield, PA, USA) critical point drier. Dried membranes were then mounted onto 12 mm SEM stubs using carbon adhesive and coated with gold using a Cressington 108Auto (Cressington, Watford, UK) sputter coater. Cells were then observed using a FE-SEM Zeiss SIGMA 300 (Carl Zeiss Microscopy GmbH, Jena, Germany). Measurements were realized directly with the microscope or on digital images using ImageJ software (Rasband, 1997). For measurements of the curved apical pore plate (Po), the arc length was measured in apical view.

2.4 DNA amplification and sequencing

For DNA amplification, direct cell PCR approach was applied using single cells from bloom sample fixed in Lugol's solution, or a few cells from the cultures in early exponential growth phase preserved in ethanol 70%. Under the inverted microscope, fixed cells were pipetted and rinsed in several drops of nuclease-free distilled water, and then transferred into a 0.2 mL PCR tube.

Due to the low amount of DNA, a first round of PCR was realized using ITS-FW (Nézan et al., 2014) and Dino-RB (5'-TTGGGACTTCTGCGTCTCAA-3', this study) primers, allowing the amplification of the ITS1–5.8S rDNA region (ITS1–5.8S–ITS2), LSU rDNA D1–D3 and D8–D10 regions. A second round of PCR (nested PCR) was realized using 1 µl of the amplicon produced in the first step as template. Primers used for the second amplification are given in Nézan et al. (2014) and Chomérat et al. (2019). PCR reactions were realized in 20 µL using KOD Hot Start Master Mix (Novagen-Merck KgaA, Darmstadt, Germany), according to the manufacturer's instructions. For both PCR rounds, the cycling conditions comprised an initial 2 min heating step at 95°C to activate the polymerase, followed by 30 cycles of 95 °C for 20 sec, 50 or 56 °C depending on primers, for 20 s, and a final extension at 70 °C for 150 sec. Prior to sequencing, amplicons were visualized on an agarose gel after electrophoresis and the positive samples were purified using the ExoSAP-IT PCR Product Cleanup reagent (Affymetrix, Cleveland, OH, USA).

For sequencing of the amplicon generated at the second PCR round, the Big Dye Terminator v3.1 Cycle Sequencing Kit (Applied Biosystems, Tokyo, Japan) was used after removal of the primers and excess dye-labeled nucleotides using the Big Dye X-terminator purification kit (Applied Biosystems, Foster City, CA, USA). Sequencing products were run on an ABI PRISM 3130 Genetic Analyzer (Applied Biosystems). Forward and reverse reads were obtained.

2.5 Alignment and phylogenetic analyses

For the three genetic markers studied, parameters of the matrices used for phylogenetic analyses are given in Supplementary Table S1. Alignments were realized using the MAFFT algorithm with the selection of the q-ins-i strategy (Kato and Standley, 2013).

Prior to phylogenetic analyses, the search for the most appropriate model of sequence evolution has been performed using jModeltest2 v. 2.1.7 (Darriba et al., 2012). Two methods of phylogenetic

reconstruction were used. Maximum Likelihood analysis (ML) was performed using PHY-ML v. 3 software (Guindon et al., 2010), and a bootstrap analysis (1000 pseudoreplicates) was used to assess the relative robustness of branches of the ML tree. Bayesian Inference analysis (BI) was realized using MrBayes 3.1.2 software (Ronquist and Huelsenbeck, 2003). Parameters of the models for ML and BI analyses are given in Supplementary Table S1.

Genetic distance (uncorrected genetic p distance) calculations among and within the *Ostreopsis* clades were estimated from the LSU rDNA D8–D10, LSU rDNA D1–D3 and ITS–5.8S rDNA matrices used for phylogenetic analyses, using the p -distance model in MEGA X: Molecular Evolutionary Genetic Analysis across Computing Platforms v. 10.0.5 (Kumar et al., 2018). Gaps and missing data were treated with the pairwise deletion option in MEGA X.

2.6 Toxicity analysis

2.6.1 Extraction procedures

The field sample (bloom) and eight clonal strains of *Ostreopsis* were further tested for their toxicity. Aliquots of 15 mg of freeze-dried cultured cell pellets corresponding to a total cell biomass $\approx 10^6$ cells, and 50 mg of the freeze-dried field sample were extracted under sonication in 670 μ L of methanol (MeOH)/water (1:1, v/v) for 15 min in an ice bath. Once cell disruption was completed, the sample was centrifuged at 10,000 g at 4 °C for 10 min. The resulting supernatant was carefully recovered and the cell pellet extracted again in 670 μ l of MeOH/water (1:1, v/v). Both supernatants were pooled (total volume recovered: ≈ 2 mL) and centrifuged at 10,000 g at 4 °C for 15 min. Finally, a 1.6 mL aliquot was sampled, evaporated to dryness at room temperature under nitrogen flux, and weighed. Supplementary Table S2 gives dry extract weight (DEW) obtained for each dry extract following this extraction step. Each dry extract was resuspended in MeOH/water (1:1, v/v) at a concentration of 10 mg·mL⁻¹ and stored at -20°C until tested for further toxicity analyses.

2.6.2 Neuroblastoma cell-based assay (CBA-N2a)

The toxicity of *Ostreopsis* samples was assessed using the CBA-N2a following the protocol previously described in Chomérat et al (2019). First, a qualitative screening was performed by testing each extract at a unique concentration of 47,619 ng·mL⁻¹ (corresponding to 10 µL of a 1:10 dilution of each dry extract stock solutions) in the absence vs. presence of 200 µM ouabain (final concentrations) (O⁻ and O⁺ conditions, respectively), each point run in triplicate in a single experiment. Next, quantitative CBA-N2a analyses were conducted only on extracts showing a cytotoxic activity. For each toxic extract, eight distinct concentrations ranging from 8.7 to 19,047.6 ng·mL⁻¹ for cell samples and 4.4 to 9,523.8 pg·mL⁻¹ for a standard of PITX (Wako, Ref. 165-26141) were tested in triplicate in three independent experiments, to obtain full dose-response curves. Following a 20–22 h incubation period, cell viability was assessed using 3-(4,5-dimethylthiazol-2-yl)-2,5-diphenyl tetrazolium bromide (MTT) assay according to Darius et al. (2018). Resulting coloration was measured at 570 nm on a plate reader (iMark Microplate Absorbance Reader, BioRad, Marnes-la-Coquette, France). One microplate in three independent experiments were examined for the purpose of inter-assay variability comparison, allowing the calculation of coefficient of variation (CVs).

For each quantitative CBA-N2a, the absorbance data for PITX standard and cell extracts were fitted to a sigmoidal dose-response curve (variable slope) based on the 4-parameter logistic model (4PL), allowing the calculation of EC₅₀ values defined as the concentration inducing 50% of viability between the top and bottom of the curve, using Prism v8.1.2 software (GraphPad, San Diego, CA, USA). The toxicity (T) of *Ostreopsis* sp. 6 samples (expressed in pg PITX equiv. cell⁻¹) was estimated using the following formula: $T = (EC_{50,PITX}/EC_{50,sample}) \times (DEW/\text{total biomass analyzed})$.

2.6.3 Liquid Chromatography coupled with tandem Mass Spectrometry (LC-MS/MS)

Aliquots of the aqueous methanolic extracts from the 8 strains and 1 field sample used for the CBA-N2a test were screened for the presence of PITX and related known structural analogues at Ifremer Phycotoxins Laboratory (Nantes, France). After resuspension in MeOH 50%, extracts were ultrafiltered (0.20 μm , Nanosep MF, Pall, Mexico). LC-UV-MS/MS analyses using the MRM (Multiple Reaction Monitoring) mode of acquisition were conducted as in Chomérat et al. (2019) with minor modifications. In total, two LC-MS/MS and one LC-UV-MS/MS methods were used to detect PITX, 42-OH-PITX, 12 OvTXs (-a to -k), 4 OSTs (OST-A, -B, -D and -E1), 3 McTXs (A to C) and OTX-1 and -3.

A focus was performed on OSTs and the following precursors giving fragment A (m/z 313.2) were added: m/z 1317.2; 1309.2; 1300.2 and 878.5; 873.1; 867.1 (corresponding to $[\text{M}+2\text{H}-\text{H}_2\text{O}]^{2+}$ and $[\text{M}+3\text{H}-\text{H}_2\text{O}]^{3+}$ ion species for OST-A/-B, -D and -E1, respectively).

To confirm the identity of OSTs, we used both the EPI (Enhanced Product Ion) mode of acquisition on the $[\text{M}+2\text{H}-\text{H}_2\text{O}]^{2+}$ and $[\text{M}+2\text{H}]^{2+}$ precursors (CE = 20 eV) and LC-HRMS (High Resolution Mass Spectrometry) as in Georges des Aulnois et al. (2019).

3. Results

3.1 Morphology of *Ostreopsis* cells

Microscope observations of fresh samples revealed the bloom was dominated by *Ostreopsis* cells, although assemblages of diatoms dominated by *Haslea* sp. were also visible (Fig. 2D).

The shape of *Ostreopsis* cells from strain PNA19-9 and wild sample varied from typical tear-shaped (pointing ventrally) to almost round in apical and antapical views (Figs 3A–B, D–E, 4A–D). They were biconvex, flattened and undulated, with the cingulum slightly sigmoid in lateral view

(Figs 3C, G, H, 4E–I). Cells from wild sample were 58.0–82.5 μm (mean 71.5 μm ; s.d. 4.5 μm , $n = 30$) deep (dorso-ventral length, DV) and 45.7–61.2 μm (mean 51.2 μm ; s.d. 3.3 μm , $n = 25$) wide (width, W). The DV/W ratio was 1.1–1.5 (mean 1.4; s.d. 0.1, $n = 23$).

The thecal plate pattern was APC 3' 7'' 6c 4's 5''' 2''''', and thecal plates were clearly visible both with light epifluorescence microscopy on strain PNA19-9 (Fig. 3D–I) and SEM on the field sample (Figs 4A–I, 5A–J). The apical pore complex (APC) consisted in a narrow, elongated and slightly curved Po plate (Figs 5A–B) bearing a slit and two rows of pores. It was located parallel to the left mid-lateral to dorsal cell margin. The Po plate was 15.6–19.5 μm (mean 17.5 μm ; s.d. 1.1 μm , $n = 14$) long. Related to the DV length (depth) of the cell, the Po/DV ratio was 0.22–0.27 (mean 0.25; s.d. 0.02, $n = 14$). The first apical plate (1') was hexagonal, elongated, located mostly on the left side of the cell (Figs 3D, 4A, C). On its dorsal part, it is slightly protruding over the APC (Figs 4A, 5A–B). The second apical plate (2') was narrow and elongated, and located below the APC, extending dorsally the Po plate and reaching the precingular plate 4'' (Figs 3I, 4H, 5A–B). The third apical plate (3') was pentagonal in shape, in contact with 1', 2', 4'', 5'' and 6'' but also had a very short contact with Po plate (Figs 4A, 5A–B). Of the precingular series, 1'' plate was the smallest while 6'' plate was the largest (Figs 3D, 4A, C). All precingular plates were four-sided except 2'' and 6'' plates that were pentagonal (Fig. 4A). The cingulum was narrow, slightly descending and undulated (Figs 3C, G, 4E–I). In the ventral view, the cingulum appeared with a V shape (Fig. 4E–F) while it was slightly sigmoid in lateral views (Figs 3G–H, 4H–I). The postcingular plate series comprised 5 plates (Figs 3E, 4B, D), 1''' being small and more conspicuously visible ventrally and laterally (Fig. 4E–H). The remaining four postcingular plates were large (Figs 3E, 4B, D). Among postcingular plates, 1''' was three-sided (Figs 4E, G–H, 5D), 2''' five-sided, and 3''', 4''' and 5''' four-sided (Fig 4B, D, H–I). The two antapical plates were unequal in size, 1'''' plate being small and covering part of the sulcus, while 2'''' plate was elongated, oriented in a slightly oblique direction in

regard with the dorsoventral axis, and with its sutures with 2^{'''} plate and 5^{'''} plate nearly parallel (Figs 3E–F, 4B, D).

The cingulum consisted of 6 distinct plates not studied in detail (Fig. 4H–I). The sulcus was studied partially and four plates only could be observed. The posterior sulcal plate (Sp) was small and roughly pentagonal, in contact with the posterior right sulcal plate (Sdp), 5^{'''} plate, 2^{'''} plate and overlapped by 1^{'''} plate (Fig. 5D–G). The anterior right sulcal plate (Sda) contacted at least six plates, including last cingular plate c₆ (Fig. 5E–G). It formed a conspicuous thick list oriented obliquely to the left along its suture with the anterior left sulcal plate (Ssa), below the ‘ventral opening’ (Vo) (Fig. 5C–G). This round opening with a thick border was 1.2–1.8 μm in diameter, and consisted in deep indentation with a Latin upsilon letter shape within Ssa plate, closed anteriorly by the epithelial 1^{''} plate (Fig. 5E–G). Another plate (Sdp), seen partially as a narrow extension without any thecal pore, was present between Sp and Sda plates (Fig. 5E–G). The presence of other platelets could not be revealed due to the overlap by the 1^{'''} plate (Fig. 5G).

The thecal surface was smooth and plates possessed pores of two kinds. Large pores were numerous, scattered all over thecal plates and well visible in LM (Figs 3F, 4A–I, 5A–I). They consisted in round pores 0.34–0.65 μm in diameter (mean 0.46 μm; s.d. 0.07 μm; *n* = 31), surrounded by small depressions in the plates forming like a rim on the edge of the pore (Fig. 5A–B, H, I). This feature was not visible from the inside (Fig. 5J). Small pores, 49–80 nm in diameter (mean 66 nm; s.d. 8 nm; *n* = 31) were sparsely scattered on the surface of thecal plates (Fig. 5A–B, H–I) but appeared more numerous on the internal side (Fig. 5J). A density of approximately 6.9 (5.4–7.8) and 7.4 (4.1–10.9) pores per 100 μm² (calculated on five specimens) was observed for large and small pores, respectively. As it is generally the case, the small pores could not be seen in LM and epifluorescence microscopy due to their small size (Fig. 3F).

3.2 Molecular phylogenies

For the phylogenetic analyses inferred from LSU rDNA D8–D10, D1–D3, and ITS-5.8S sequences, a total of 14, 6, and 6 new sequences from Tahiti, French Polynesia, as well as reference sequences retrieved from GenBank, were used (i.e. LSU rDNA D8–D10: IFR19-631/IFR20-173 to -178, and PNA19-1 to -4/PNA19-6 to -9 acquired from six single cells isolated from the wild bloom and eight cultured strains, respectively; LSU rDNA D1–D3 and ITS-5.8S: IFR20-173 to -175 and PNA19-6, -8 and -9 acquired from three single cells isolated from the wild bloom and three cultured strains, respectively). Parameters of the alignment and model chosen for the analyses are summarized in Supplementary Table S1.

Both analyses performed with ML and BI gave the same tree topology and identical relationships among *Ostreopsis* clades. Hence, only the majority-rule consensus trees of the ML analyses are shown (Figs 6, 7, 8).

3.2.1 LSU rDNA D8–D10 regions

All 14 sequences acquired from Tahiti clustered within *Ostreopsis* sp. 6 which was a well-supported clade (ML = 98, BI = 1.00), sister to *O. lenticularis* (Fig. 6). Sequences acquired from single cells of the bloom and cultured strains were nearly identical and clustered in a new subclade A of *Ostreopsis* sp. 6 (Fig. 6). This subclade of 14 sequences corresponded to a sister clade of two sequences from Thailand (strains TF29OS and TF25OS, subclade B) with a moderately high support (ML = 95, BI = 0.90). Two sequences from Japan (strains s0587 and s0595, subclade D) branched with a strong support (ML = 96, BI = 1.00) at the base of the subclades A and B. Another group of five sequences from Japan (OU8, IR33, IR49, and OU11) and Korea (17JJ0906) formed a subclade E which appeared as a sister clade to the subclades A, B, and D with a moderate support (ML = 96, BI = 0.66) (Fig. 6).

A low genetic divergence was observed within each subclade, with p -distances varying from 0.000 (subclade A) to 0.002 (subclade C, Table 1). The p -distances between subclades showed the subclades A (Tahiti) and B (Thailand) were the most closely related with a p -distance of 0.002. In contrast, the subclades D and E (Japan/Korea) appeared more divergent from other subclades A and B with p -distances of 0.012 to 0.013 (Table 1).

3.2.2 LSU rDNA D1–D3 regions

The 6 sequences acquired from the Punaauia bloom clustered within *Ostreopsis* sp. 6 which was a fully supported clade (ML = 100, BI = 1.00), sister to *O. lenticularis* (Fig. 7). The six sequences from Tahiti formed a well-resolved subclade A within *Ostreopsis* sp. 6 (ML = 90, BI = 0.96), and two sequences from Malaysia (OIPR01, subclade B) and Viet Nam (NT013, subclade C) appeared closely related and more basal (Fig. 7). These eight sequences formed a well-supported subclade of *Ostreopsis* sp. 6 (subclades A-C) (ML = 88, BI = 1.00), and three sequences from Japan (OA21, subclade D/E?) formed a sister clade with a maximal support (Fig. 7). In absence of other sequences for other markers allowing comparisons with subclades D and E, sequences of strain OA21 are putatively ascribed to ‘D/E?’.

A low genetic divergence was observed within each subclade, with p -distances varying from 0.001 (subclade A) to 0.023 (subclade D/E?, Table 1). The p -distances between subclades showed the subclades A (Tahiti) and B (Malaysia) were the most closely related with a p -distance of 0.032. In contrast, the subclades C (Viet Nam) and D/E? (Japan) appeared more divergent from subclades A and B with p -distances of 0.046 to 0.105 (Table 1).

Of note, there is currently no reference sequence for D1-D3 LSU rDNA from the Gulf of Thailand whereas only one sequence (in same subclade B with ITS–5.8S rDNA region) ascribed to ‘*O. lenticularis*’ (already mentioned) is presently available from Malaysia (OIPR01) (Fig. 7).

3.2.3 ITS–5.8S rDNA phylogeny

All the 6 sequences acquired from Tahiti clustered as a basal subclade A within *Ostreopsis* sp. 6 (Fig. 8). The most closely related sequences were in subclade B which included two sequences from Thailand (TF29OS and TF25OS) and two from Malaysia (OlPR01 and VGO87, Fig. 8). Two sequences from Viet Nam (NT011 and NT012) were more divergent and included in the subclade C, while three sequences from Japan (s0587, IR33 and OU11) formed the subclades D and E, but support was low (Fig. 8).

Except for the subclade E, a low genetic divergence was observed within each subclade, with *p*-distances of 0.002 (subclade A), 0.004 (subclade B) and 0.008 (subclade C, Table 1). The *p*-distances between subclades showed the lowest *p*-distance was observed between the subclade A (Tahiti) and B (Thailand/Malaysia) with a value of 0.008. In contrast, the subclade A was more divergent from the subclades D (*p*-distance 0.147) and E (*p*-distance 0.127), including sequences from Iriomote and Okinawa islands, Japan (Table 1).

3.3 Toxicity and toxin analyses

3.3.1 Toxicity analyses using the CBA N2a

At the screening step, no toxicity was detected in the field sample, whereas all eight strains tested were found toxic in O⁻ and O⁺ conditions. When doing quantitative analyses, the PITX standard displayed a dose-response curve with a vertical negative slope in O⁻ conditions and a sigmoidal dose-response curve with a negative slope in O⁺ conditions, giving EC₅₀ values of 1,074 ± 23 and 156 ± 17 pg·mL⁻¹ (*n* = 3), respectively (Fig. 9A). The composite toxicity of the eight strains of *Ostreopsis* sp. 6 showed a pattern similar to that of PITX standard (Fig. 9B). The

estimated toxin contents ranged from 1.73 ± 0.31 to 2.48 ± 0.22 pg PITX equiv. cell⁻¹ in O⁻ conditions ($n = 3$), and from 1.08 ± 0.09 to 1.40 ± 0.14 pg PITX equiv. cell⁻¹ in O⁺ conditions ($n = 3$) (Table 2). A good reproducibility of toxin contents was observed between experiments, with coefficients of variation (CVs) ranging from 4.2 to 17.8 % in O⁻ conditions and from 2.9 to 10.6% in O⁺ conditions (Table 2). Comparison of the toxicity data between strains indicate slight differences, with a mean toxicity of 2.16 ± 0.25 and 1.27 ± 0.12 pg PITX equiv. cell⁻¹ in O⁻ conditions (CV of 11.5%) and O⁺ conditions (CV of 9.2%), respectively. Of note, the curves obtained in O⁺ conditions showed the best agreement with the 4PL model used in Graphpad software, so only these values should be considered for further comparison with the toxicity data available in the literature.

3.3.2 Analyses by LC-MS/MS

Among the PITX-like compounds screened for, we could detect OSTs in the eight strains cultivated but not in the field field sample (Supplementary Fig. S1). Total OSTs varied from 21 to 28 pg PITX equiv. cell⁻¹ (Fig. 10). The OST profile was dominated by OST-D (>90%) followed by OST-A and -B in all strains tested.

As no OST standard is commercially available, we tried to confirm the identity of OSTs by both low and high resolution mass spectrometry. While EPI scan confidently proved the identity of OST-D (Fig. S2) when compared to fragments reported by Terajima et al. (2018a), the intensity for the other analogs was unfortunately too low. In addition, exact masses obtained by HRMS analyses unambiguously confirmed the presence of OST-A and -B (Δ ppm: -3.1 to +1.9, Fig. S3). The HRMS spectra showed a characteristic pattern, with the forms $[M+2H-H_2O]^{2+}$ and $[M+H+Na]^{2+}$ being more abundant. However, the $[M+H+Na]^{2+}$ exact mass corresponding to OST-E1 was missing, suggesting its absence in the OST profile of the strains studied here. Finally, as OST-A and -B are isomers and

due to the absence of a published chromatogram, their identity was defined based on their retention time (OST-A eluting first).

4. DISCUSSION

4.1 Phylogeny and taxonomy of the bloom forming species from Tahiti Island

4.1.1 Phylogenetic position

Molecular data and phylogenetic analyses revealed that the species responsible for the bloom belongs to the *Ostreopsis* sp. 6 clade, originally proposed by Sato et al. (2011) and subsequently used by several authors (Tawong et al., 2014; Zhang et al., 2018; Chomérat et al., 2019; Lee and Park, 2020). So far, this genotype has been found in various areas of southwestern Asia, including the Gulf of Thailand, especially at the TF site (Tawong et al., 2014) which corresponds roughly to the type locality of *O. siamensis* Johs. Schmidt, in Malaysia (subclade B), Viet Nam (subclade C), and several islands of Japan (subclades D-E; Sato et al., 2011). Very recently, Lee and Park (2020) reported the presence of this species (subclade E) in the subtropical area of Jeju island, South Korea, which is the northernmost record to date. Hence, the present study is the first report of this species from the mid-Pacific area. Genetic distances among the different subclades revealed that there are some divergences between the subclades, suggesting that *Ostreopsis* sp. 6 might actually represent a complex of closely related species, as is the case for the *O. cf. ovata* clade. Nevertheless further studies will be necessary to resolve this issue.

Sequences from French Polynesia (subclade A) appeared more closely related to the sequences from the Gulf of Thailand/Malaysia (subclade B in present analyses), than to sequences from other origins (Viet Nam, Japan, Korea: subclades C, D and E). Consequently, the low genetic divergence between subclades A and B can likely be interpreted at an intraspecific level. For instance, the ITS–5.8S region sequences of subclades A and B diverged by 0.008 which is much lower than the

threshold value of 0.04 proposed by Litaker et al. (2007) to separate two given dinoflagellate species. In contrast, the sequences from Viet Nam and Japan (subclades C, D, E) were more variable and divergent from subclades A and B (ITS *p*-distances exceeding 0.04), which suggest they likely represent different species. Nevertheless, more detailed studies including comparisons of the ITS2 secondary structure of the different ribotypes would be necessary to resolve this question in the future.

4.1.2 Identity of *Ostreopsis* sp. 6

In previous studies, the clade *Ostreopsis* sp. 6 was left unnamed since the morphology of the strains was not studied or confusing. By way of example, the phylogeny inferred from ITS–5.8S region includes two sequences from Malaysia originally ascribed to *O. labens* M.A. Faust & S.L. Morton (VGO897) and *O. lenticularis* (OIPR01), respectively. Of note, this latter identification later proved erroneous since strain OIPR01 clusters within *Ostreopsis* sp. 6 and not with *O. lenticularis* (Chomérat et al., 2019). Moreover, these sequences were almost identical to sequences from the Gulf of Thailand (TF25OS and TF29OS) which likely correspond to *O. siamensis* since they were acquired from the area studied by Schmidt (1901), near Koh Wai Island. Although Tawong et al. (2014) did not provide a detailed morphological SEM description of strains TF29OS and TF25OS, they reported a dorsoventral (DV) length (= depth) size range of 49.9–84.3 μm for TF29OS, and also highlighted a conspicuous undulated shape in lateral view (Fig. 4 in Tawong et al., 2014). This feature is typical of *O. siamensis* as showed by Schmidt (1901) although this author mentioned a DV length of 90 μm without any indication of the size variation range. Morphological features of strain TF29OS appears in good agreement with the original description but, unfortunately, it has been lost (T. Nishimura, pers. comm.), so further investigations to clarify whether it could be ascribed to *O. siamensis* or not, is no longer possible. However, since genetic data clearly show that

strains from the Gulf of Thailand and those from Tahiti Island (subclades B and A, respectively) belong to the same species, the present morphological data are therefore useful to complete the previous study by Tawong et al. (2014).

The specimens from the bloom at Toaroto beach, Tahiti were in the same size range than those reported for strain TF29OS by Tawong et al. (2014). The larger DV length (depth) mean value found in the present study (71.5 μm vs. 62.4 μm in Tawong et al., 2014) can easily be interpreted by our observation of field specimens from the bloom (i.e. a natural population) while Tawong et al. (2014) values were obtained from a culture. Although the size is lower than the value from the original description by Schmidt (1901), it fits perfectly with the interpretation of *O. siamensis* by Fukuyo (1981) who gave a DV length range of 60–100 μm . The single value reported by Schmidt (1901) should be considered cautiously and is likely due to the low cell densities in the plankton samples he examined at station 2 (between Koh Kahdat and Koh Kut), and even lower densities found at stations 3 and 6 (South of Koh Chang). Moreover, cell specimens from the bloom and strains from Tahiti displayed a variable outline, from almost round to tear-shaped, consistent with the original drawings by Schmidt (1901). Several authors (e.g., Accoroni and Totti, 2016) hypothesized that these drawings could well represent different taxa with different shapes but this hypothesis likely results from a misinterpretation of the shape as a distinctive feature between *O. siamensis* and *O. lenticularis*. As noted previously, Fukuyo (1981) never indicated that the outline can distinguish these species (Chomérat et al. 2019). The present data confirm that such variability exists in *Ostreopsis* sp. 6, both in a field sample and in cultured strains.

Additionally, the undulated (slightly sigmoid) cingulum observed in the specimens from Tahiti Island is in good agreement with the report by Tawong et al. (2014). This remarkable feature, resulting in a slightly concave hypotheca, fits extremely well with the original drawings (Fig. 7 in Schmidt, 1901) and with the description indicating an ‘inferior valve a little concave’ (Schmidt, 1901).

The presence of conspicuous thecal pores was confirmed on the specimens from Tahiti, where larger thecal pores had a diameter of 0.34–0.65 μm , as reported for TF29OS (Supplementary Table S2 in Tawong et al., 2014). This large size makes them perfectly visible in light microscopy, which is again consistent with the drawings by Schmidt (1901) and interpretation of *O. siamensis* by Fukuyo (1981). However, our study also showed the presence of very small thecal pores that are impossible to resolve in LM, which may explain their absence both in the original description and re-interpretation of *O. siamensis* (Schmidt, 1901; Fukuyo, 1981), but also in the study by Tawong et al. (2014).

However, our observations do show several discrepancies compared to the original description of *O. siamensis* with regard to the APC and the second apical plate 2'. In the original drawing, the APC appeared rather short compared to the DV length (depth) of the cell (Po/DV of 0.22 measured in Schmidt's Fig. 5) while slightly larger values were found in our study. In comparison, Tawong et al. (2014) indicated a Po plate length of 16 μm in their Supplementary Table S2, which is in the lower range of our observations. Using the average DV value, the Po/DV of strain TF29OS was 0.26, which is in the range found in the present study. Furthermore, the apical 2' plate appeared to be short, and nearly of the same length as Po plate in Fig. 5 by Schmidt (1901). This seems in marked contrast with our observations which described a narrow and very elongated 2' plate reaching the dorsal precingular plate 4". Such a long 2' plate was reportedly observed only in *O. heptagona* and the recently described species *O. fattorussoi* and *O. rhodesiae* (Norris et al., 1985; Accoroni et al., 2016; Verma et al., 2016a). This is no longer true since extensive observations on *O. cf. ovata* have revealed that several populations also display a long 2' plate (Besada et al., 1982; Parsons et al., 2012; Tibirićá et al., 2019). Moreover, in the largest species of the genus, *O. mascarenensis*, our previous study showed that the 2' plate is actually long and it reaches 4" plate (Chomérat et al., 2020), which contradicts the original description by Quod (1994). All these findings suggest the actual shape of this plate was probably overlooked in previous studies. In *O.*

siamensis, Fukuyo (1981) interpreted a small, long and narrow 2' plate as reported in the original drawing by Schmidt (1901), but the exact shape and length are not clearly visible from LM pictures. So whether the 2' plate was actually short in the population or the interpretation was influenced by the original description could not be determined. As previously emphasized by Chomérat et al. (2020), the study of this plate is extremely difficult due to its narrowness and recessed position below the APC. The relevance of this plate has also significantly increased with the descriptions of new *Ostreopsis* species characterized by rather close plate pattern. Indeed, the need to identify consistent diagnostic features and the development of more and more powerful techniques such as epifluorescence or SEM has rendered the study of the APC and 2' plate more prominent in modern taxonomy. When Schmidt (1901) described *O. siamensis*, the morphology of this new genus was so unusual and different from all other known dinoflagellates, that there was probably no need to study this tiny and recessed plate with as many details as today, therefore original drawings should be taken cautiously. To support this statement, it should be mentioned that Schiller even omitted to report the APC and 2' plate in the illustration of the genus *Ostreopsis* in his monograph (Fig. 543b in Schiller, 1937).

All the above morphological features reported for the specimens from Tahiti are in rather good agreement with the description of *O. siamensis*, and the fact that it is genetically almost identical to a strain from the type locality strongly argues in favor of this identity. Nevertheless, most of these features fit also quite well with the description of another species, *O. labens* which also has a conspicuous undulation and is very difficult to separate from *O. siamensis*. The type locality of *O. labens* is Man of war Cay, Belize but Faust and Morton (1995) indicated the presence of this species in several places from Japan (Iriomote, Ishigaki Islands) and East China, and this distribution was extended to southwestern Indian Ocean (Faust et al., 1996). The reasons why *O. labens* has been separated from *O. siamensis* are unclear, and the main difference between them appears to be the anteroposterior length reported as 60–86 μm in *O. labens* (Faust and Morton, 1995), which is higher

than for *O. siamensis* (Hoppenrath et al., 2014). Nevertheless, this feature is doubtful since it does not correspond to the illustrations provided by Faust and Morton (1995) and based on the scale bar, the cell illustrated in their Fig. 8 had an estimated width of 67 μm and an AP length of 44 μm , which is surprisingly outside the range given in the description. Hence, the diagnostic features of *O. labens* appear to be questionable, and the dimensions must be regarded cautiously. In their description of *O. labens*, Faust and Morton (1995) reported a DV length (depth) of 81–110 μm but this was surprisingly further reported to 86–98 μm one year later (Faust et al., 1996). Thus, it is mostly in the range given by Fukuyo (1981) for *O. siamensis* (60–100 μm). Moreover, as discussed earlier, Faust et al. (1996) likely made a major confusion between *O. siamensis* and *O. lenticularis* and all their data reported for ‘*O. lenticularis*’ (our quotation marks) actually fit better with *O. siamensis*, while the data for ‘*O. siamensis*’ concern *O. lenticularis* (Chomérat et al., 2019). According to Faust et al. (1996), ‘*O. lenticularis*’ (likely *O. siamensis*) has a DV length of 65–75 μm which is not only in the range given by Fukuyo (1981) for *O. siamensis* but also in the range of *Ostreopsis* sp. 6 [strain TF29OS (Tawong et al., 2014) and field cells observed in the present study]. Unfortunately, Faust et al. (1996) did not report the AP length for this species, preventing any further comparison with *O. labens*. Except for size, no striking difference can be found between *O. labens* and ‘*O. lenticularis*’ (likely *O. siamensis*) in Faust et al. (1996). They both possess a similar thecal arrangement, an undulated cingulum (undescribed but visible on the illustrations), and large thecal pores in depressions and surrounded with a rim (Faust et al., 1996). This structure of large thecal pores is remarkably similar in *Ostreopsis* sp. 6 (e.g., Fig. 29 in Fukuyo, 1981; Fig. 2H in Lee and Park, 2020, present study), *O. labens* and ‘*O. lenticularis*’ (Faust and Morton, 1995; Faust et al., 1996), indicating their probable taxonomic proximity and possible conspecificity. The presence of very small thecal pores observed in the present study may have been overlooked in older studies since these pores are rare on the cell surface and they require that the amphiesmal and cell

membranes to be well removed. In any case, these small pores are impossible to see in LM, and their scarcity on thecal plates makes a major difference from *O. lenticularis* (Chomérat et al., 2019).

In the light of the molecular data showing that *Ostreopsis* sp. 6 encompasses cryptic diversity, one of the subclades D or E might correspond to *O. labens* since Faust and Morton (1995) designated paratypes from Iriomote and Ishigaki islands, Japan. Phylogenetic analyses revealed that great diversity exists at Iriomote-Kohama-Ishikagi Islands which are part of the Ryukyu archipelago, and sequences clustering in the subclades D and E are both present. Since Fukuyo (1981) studied specimens from this area, he may have reinterpreted *O. siamensis* in a broad sense, encompassing cryptic (or pseudocryptic) species within *Ostreopsis* sp. 6, and possibly *O. labens*. However, to confirm this hypothesis and clarify the delineation of *O. labens*, additional molecular data are needed from the type locality (Man of war Cay, Belize).

The molecular data from the Gulf of Thailand and type locality of *O. siamensis* (Tawong et al. 2014), together with the detailed morphological description herein bring new evidence that the subclades A and B of *Ostreopsis* sp. 6 likely correspond to the real *Ostreopsis siamensis*, as described by Schmidt (1901). Nevertheless, in the absence of a culture of this species from the type locality in the Gulf of Thailand, it is impossible to define a neotype yet. In contrast with the recent review by Tester et al. (2020), this study demonstrates unambiguously that *Ostreopsis* sp. 6 should not be considered as a cryptic species of *O. lenticularis* (= *Ostreopsis* sp. 5), and instead, corresponds to a fully separated species, most likely *O. siamensis*. This novel report from Tahiti Island is extremely interesting as only two morphospecies are currently reported from French Polynesia so far, namely *O. ovata* and *O. lenticularis* (Fukuyo, 1981; Chomérat et al., 2019). In his study, Fukuyo (1981) clearly indicated that *O. siamensis* was not present in the samples from Tahiti and Gambier Islands.

4.1.3 Taxonomic comparison with '*Ostreopsis cf. siamensis*' from temperate locations

The nomenclatural combination '*Ostreopsis cf. siamensis*' has been used to designate a clade that includes sequences from the Mediterranean, Atlantic-Iberian peninsula, northern New Zealand, Russia and Australia which all classify in temperate (Cf) to warm Mediterranean climates (Csa) and subtropical humid (Cwa) according to the Köppen-Geiger climatic classification (Table 3, Peel et al., 2007; Beck et al., 2018). In contrast with *Ostreopsis* sp. 6 for which genetic divergence is relatively high and may indicate the existence of cryptic species, molecular data for '*O. cf. siamensis*' show a lower level of variation among populations from the different temperate areas. Hence '*O. cf. siamensis*' can be interpreted as a single species, related to *O. rhodesiae* in phylogenies, but very recently, Verma et al. (2020) showed the existence of low genetic variability and identified two subclades within '*O. cf. siamensis*' from Australia. Despite this relative genetic stability, morphology reported for this species is rather variable and sometimes conflicting features have been mentioned but it is likely that several confusions were made and the taxonomic identity was not ascertained. The lack of molecular data for previous reports from the temperate areas (e.g., the northern part of New Zealand, Chang et al., 2000; Rhodes et al., 2000) prevents to clarify their actual identity and morphological data were not detailed enough to conclude. Nevertheless, it is likely the same temperate species that clusters in the clade '*O. cf. siamensis*' since it was found in the northern part of New Zealand for which genetic data have been further acquired (Sato et al., 2011). In contrast, the species identified morphologically as *Ostreopsis cf. siamensis* by Holmes et al. (1988) from subtropical Australia (Heron and Lady Elliot islands) likely correspond to another taxon, presumably *O. siamensis*, as shown by size and characters (Table 3). Although the presence of '*O. cf. siamensis*' has also recently been confirmed at Heron Island (Verma et al., 2016a) the cells had different morphological characters (Table 3). In this area of Coral Sea, which corresponds to the limit of the tropical area, both genotypes may be sympatric. Hence, it appears that the

combination ‘*Ostreopsis cf. siamensis*’ may have been used for different taxa and is highly confusing.

As summarized by Verma et al. (2016b), the sizes reported for temperate specimens (excluding all reports from tropical waters that likely correspond to other species, Table 3) were quite variable, depending on whether observations used cultured material or field fixed specimens. The DV length varied between 34 μm (e.g., cultured cells from Merimbula, Australia, Verma et al., 2016b), to 90 μm (e.g., field specimens from the Mediterranean Sea, Penna et al., 2005). This suggests that size is a poor taxonomical character to distinguish temperate ‘*O. cf. siamensis*’ from tropical *O. siamensis* and *Ostreopsis* sp. 6 due to the overlap (Table 3). Besides, as for almost all *Ostreopsis* species, the plate pattern does not exhibit any major difference (Parsons et al., 2012). Interestingly, in their Fig. 2f, Verma et al. (2016b) illustrated a short 2' plate, not reaching the precingular 4" plate, very similar to Schmidt's illustration, but their SEM micrograph of the 2' plate (cf. Fig. 3c in Verma et al., 2016b) is not clear and seems to indicate a contact between 2' and 4" plates. In contrast, Selina and Orlova (2010) and David et al. (2013) illustrated a conspicuously long 2' plate, as shown in our study. Consequently, the length of 2' plate does not constitute a good character to distinguish ‘*O. cf. siamensis*’ from *Ostreopsis* sp. 6 and it appears necessary to reinvestigate this feature for all *Ostreopsis* species as the interpretation may have been mistaken.

Two important features should be better evaluated for the discrimination of species from the tropical area (*O. siamensis* / *O. labens*/ *Ostreopsis* sp. 6) from the more temperate ‘*O. cf. siamensis*’. The first feature seems to be the cingulum undulation, which is conspicuous in the original description of *O. siamensis* and the present study of *Ostreopsis* sp. 6. As shown in Table 3, when studied carefully, the conspicuous undulation is found in tropical populations of *O. siamensis*, *O. labens*, and *Ostreopsis* sp. 6 whereas in populations of ‘*O. cf. siamensis*’, this feature has been rarely emphasized. Several authors indicated that cells were flat and not undulated (Penna et al., 2005; David et al., 2013; Verma et al., 2016b) while Aligizaki and Nikolaidis (2006) reported that

cells were sometimes undulated. The undulation showed in Fig. 4A by Aligizaki and Nikolaidis (2006) appears very faint and roughly similar to the observations by Selina and Orlova (2010). Nevertheless, in these studies, the illustrations do not show the same degree of undulation as illustrated by Schmidt (1901) or shown in the present study. Consequently, the degree of undulation may constitute a good feature to separate temperate '*O. cf. siamensis*' from the tropical *O. siamensis* / *Ostreopsis* sp. 6. Additionally, thecal pores may constitute another important taxonomic feature, to help separate these taxa. As shown in Table 3, the size of large and small thecal pores may be an interesting feature to consider, although this is variable among populations. It is striking that large thecal pores have the same size in *Ostreopsis* sp. 6 from the Gulf of Thailand (Tawong et al., 2014) and Tahiti (this study). This large size (0.4–0.7 μm) compares well with Schmidt's statement that plates are coarsely porous, like that of '*Ceratium tripos*' (Schmidt, 1901), who observed them only with LM. From the original drawings (cf. Fig. 6 in Schmidt, 1901), the thecal pores illustrated on the hypotheca have a roughly estimated size of 0.6–0.7 μm , considering the DV length of the cells *ca.* 90 μm . As observed in the present study, rounded cells were generally much smaller, and in absence of a scale bar in the original description, the pores size could not be estimated from the epitheca (Fig. 5 in Schmidt, 1901), or some exceed 1 μm if the DV is considered to be 90 μm . By contrast, the values for '*O. cf. siamensis*' appear lower in all studies. Penna et al. (2005) made extensive measurements of thecal pores of *O. cf. siamensis* from the Mediterranean Sea, but despite a large range of variation of 0.11–0.55 μm , the predominant size was 0.2–0.4 μm which is below the measurements in *Ostreopsis* sp. 6 (Tawong et al., 2014; this study). In addition to the size, the structure of these pores, with a depression and collar rim around the opening appears conspicuous in *Ostreopsis* sp. 6, but it has never been shown in the temperate '*O. cf. siamensis*' which has simple pores without collar rim. Thus, this feature should be further considered to separate these species.

Therefore, in the light of the phylogenetic data presently available and the morphological data from the present study, we conclude the name *O. siamensis* should be used for a species within the

clade *Ostreopsis* sp. 6 (putatively the subclades A and B), while there is a need to rename '*O. cf. siamensis*' from temperate areas since this designation is a source of additional confusion in the complex taxonomy of *Ostreopsis*.

4.2 Toxicity and toxin profiles

As previously found by Pawlowicz et al. (2013), Cañete and Diogène (2008) and Kerbrat et al. (2011), the cytotoxic effect of PITX on N2a cells was enhanced by the presence of ouabain which is in marked contrast with Ledreux et al. (2009) who concluded in a protective effect of ouabain against PITX action. In French Polynesia, the composite toxicity detected by CBA-N2a showed that all the strains isolated from the bloom were toxic in O⁻ and O⁺ conditions with a mean production of at least 1.27 pg PITX equiv. cell⁻¹ estimated in O⁺ condition and very little difference between the eight strains (9.2%). This composite toxicity was confirmed by LC-MS/MS analyses revealing the presence of three OST analogs in all strains of *Ostreopsis* sp. 6 from Tahiti: OST-A, OST-B, and OST-D, this latter composing the most important part of the toxin profile (\approx 90%). The average toxin production of the eight strains as assessed by LC-MS/MS was estimated at 25 pg equiv. PITX cell⁻¹ i.e. 19-fold higher than with the CBA-N2a. This bias could be explained by the use of PITX as the reference standard to estimate the toxin production (since OST standards are currently unavailable). The use of PITX could not allow estimating the real cytotoxic potential of these three OSTs (-A, -B and -D) on mouse neuroblastoma cells via the CBA-N2a, as-yet-unknown. Depending on the model and exposition routes, considerable differences have been found between PITX and OST-D (Ito and Yasumoto, 2009). For instance, *in vivo* experiments on mice (intra-tracheal administration) have shown that OST-D was five times less potent than PITX (Ito and Yasumoto, 2009). Using keratinocytes (HaCaT cells), Pelin et al. (2016) also noticed a lesser cytotoxicity of OST-D in comparison with PITX, and suggested that a missing hydroxyl group on C44 of OST-D, present in PITX, may cause this major difference in toxicity.

In previous studies, crude methanolic extracts of the strain s0587 (subclade D) from Haemida, South of Iriomote Island (latitude $\approx 24^\circ\text{N}$), in tropical waters of Okinawa, Japan (Sato et al., 2011) and the strain TF29OS (subclade B) from Thailand (Tawong et al., 2014) belonging to *Ostreopsis* sp. 6 and genetically closely related to the strains from Tahiti, exhibited toxicity to mice although no quantification was given. The same strain s0587 was also known to produce OST-D, around 3.5 pg PITX equiv. cell⁻¹ (Suzuki et al., 2012) using LC-MS/MS, which is *ca.* 7 times lower than for the French Polynesian strains. These levels are rather similar, albeit lower compared to other *Ostreopsis* species like *O. cf. ovata* from the northern Adriatic Sea showing high levels of PITXs up to 75 pg cell⁻¹ in natural benthic microalgal populations (Accoroni et al., 2011). Interestingly, Suzuki et al. (2012) did not detect any toxins in strains IR33 and OU11 (subclade E) of *Ostreopsis* sp. 6, which contrasts with subclades A, B and D.

Regarding the toxin profiles, the presence of OST-D as the major analogue found in the strains from French Polynesia (this study) is consistent with results obtained previously for Japanese strains, including the strain s0587 (Suzuki et al., 2012), but also with the data by Ukena et al. (2001, 2002) who isolated and purified OST-D from the strain SOA1, collected at Aka Island, Okinawa, Japan. In addition, the presence of at least three analogues within a single strain is also consistent with the recent studies of Terajima et al. (2018a, b) who purified the four OSTs known so far from the same SOA1 strain. Although this strain comes from the same island than strain OA21 (subclade D/E? in Fig. 7), no sequence has been provided for strain SOA1 which prevents a genetic comparison. Phylogenetic data suggest that there is a great diversity in the area of Iriomote-Kohama-Okinawa islands, including several genotypes of *Ostreopsis* sp. 6 (Sato et al., 2011; this study). In all phylogenetic analyses, sequences from Japan do not cluster in the same subclade as those from the Gulf of Thailand and Tahiti, which could indicate different species. Further work will thus be needed to clarify this and ascertain the presence of OST-E1 in strains from Tahiti. To date, the lack of published profiles limits further comparisons of the toxin profile found for

Ostreopsis sp. 6. Nonetheless, results obtained in this study clearly indicate that comparing toxicity and toxin composition of tropical strains of *Ostreopsis* sp. 6 with temperate strains of '*O. cf. siamensis*' (e.g., Tester et al., 2020) should be very cautious since they concern two widely divergent taxa. Such apparent conflicting reports of toxicity may result from misidentifications, and we recommend that future works on toxicity always include a molecular characterization of the strains studied to ensure their correct identification.

While all the strains isolated from the bloom exhibited toxicity, the absence of noticeable toxicity and no detection of toxins from the field sample raises questions. Since the observations of the bloom sample showed that several diatoms were co-occurring with *Ostreopsis* sp. 6, it is likely that the dried biomass represented by *Ostreopsis* cells was rather low and probably insufficient to induce a cytotoxic effect and to detect toxins. In addition, it has been shown that toxicity is highly dependent on the bloom dynamics, and Gémin et al. (2020) reported that the toxin content increased during the exponential and stationary growth phases of a bloom of *O. cf. ovata*. Hence, the toxin content per cell in the bloom at Toaroto beach could have been low if sampling was done at an early stage. In any case, further investigations will be necessary to confirm such findings, both *in situ* and in laboratory conditions, as this has major implications in terms of risk in a given area.

5. Conclusions

In the context of climate change and global warming, understanding the ecological preferences and niche of harmful benthic microalgae is an important challenge in order to predict future changes (Tester et al., 2020). Among these taxa, the genus *Ostreopsis* represents a serious threat since several species are toxic not only to human but also to marine organisms. The present observation of a bloom of *Ostreopsis* sp. 6 in French Polynesia constitutes a new record for this species since, to date, only *O. ovata* and *O. lenticularis* have been mentioned from French Polynesia (Fukuyo, 1981;

Bagnis et al., 1985; Chomérat et al., 2019). Hence, the finding of a new, toxic species, in Tahiti increases the potential risk linked to the proliferation of *Ostreopsis*. The fact that no toxicity was found in environmental samples whereas all clonal strains established from the bloom were toxic with a relatively similar profile, dominated by OST-D, raises important questions about the basis of toxin production in this species. While *O. cf. ovata* is likely the most toxic species, the risk to human populations in the Mediterranean seems manageable, but the situation may be very different in tropical areas (Tester et al., 2020). As emphasized by Deeds and Schwartz (2010), PITX-like molecules may accumulate and contaminate tropical fishes and their ingestion by humans can have dramatic health impacts, in addition to the well-known risk of CFP. Hence, further studies aiming at better evaluate the distribution of *Ostreopsis* sp. 6 in French Polynesia, and determine the ecological conditions which stimulates its proliferation now appear crucial for a better assessment of its potential impacts on the coral-reef ecosystems but also risk management purposes.

6. ACKNOWLEDGEMENTS

We thank Maurice Loir for his help in the identification of the diatoms co-occurring with the *Ostreopsis* bloom and Frederic Zentz for designing the new primer Dino-RB. The four anonymous reviewers are acknowledged for their suggestions improving significantly the manuscript. The Regional Council of Brittany, the General Council of Finistère and the urban community of Concarneau-Cornouaille-Agglomération are acknowledged for the funding of the Sigma 300 FE-SEM of the station of Marine Biology in Concarneau.

Funding

This work is part of the TATOO project and was supported by funds from the Délégation à la Recherche de la Polynésie Française (Conv. n°02400/MTF/REC of April 9th, 2018).

Authors contributions

Conceptualization : NC, MC

– Field sampling : MZ, CV, AU, KH

– Microscopy observations : NC, KH

– *in vitro* culturing : KH

– Acquisition and analysis of molecular data : NC, GB

– Acquisition and analysis of toxicity data (including extraction steps) : JV, FH, DR, AD, ZA, HTD,

MR

– Writing—original draft preparation : NC, HTD, DR, MC

– Writing—review and editing : NC, GB, JV, FH, DR, MZ, CV, CG, MR, HTD, MC

– Project supervision : MC, NC

– Funding acquisition : MC, NC

References

- Accoroni, S., Romagnoli, T., Colombo, F., Pennesi, C., Di Camillo, C.G., Marini, M., Battocchi, C., Ciminiello, P., Dell'Aversano, C., Dello Iacovo, E., Fattorusso, E., Tartaglione, L., Penna, A., Totti, C., 2011. *Ostreopsis* cf. *ovata* bloom in the northern Adriatic Sea during summer 2009: Ecology, molecular characterization and toxin profile. *Mar. Pollut. Bull.* 62, 2512–2519. <https://doi.org/10.1016/j.marpolbul.2011.08.003>
- Accoroni, S., Totti, C., 2016. The toxic benthic dinoflagellates of the genus *Ostreopsis* in temperate areas: a review. *Adv. Oceanogr. Limnol.* 7, 1–15. <https://doi.org/10.4081/aiol.2016.5591>
- Accoroni, S., Romagnoli, T., Penna, A., Capellacci, S., Ciminiello, P., Dell'Aversano, C., Tartaglione, L., Abboud-Abi Saab, M., Giussani, V., Asnaghi, V., Chiantore, M., Totti, C., 2016. *Ostreopsis fattorussoi* sp. nov. (Dinophyceae), a new benthic toxic *Ostreopsis* species from the eastern Mediterranean Sea. *J. Phycol.* 52, 1064–1084. <https://doi.org/10.1111/jpy.12464>
- Alcala, A.C., Alcala, L.C., Garth, J.S., Yasumura, D., Yasumoto, T., 1988. Human fatality due to ingestion of the crab *Demania reynaudii* that contained a palytoxin-like toxin. *Toxicon* 26, 105–107.
- Aligizaki, K., Nikolaidis, G., 2006. The presence of the potentially toxic genera *Ostreopsis* and *Coolia* (Dinophyceae) in the North Aegean Sea, Greece. *Harmful Algae* 5, 717–730. <https://doi.org/10.1016/j.hal.2006.02.005>
- Amzil, Z., Sibat, M., Chomérat, N., Gossel, H., Marco-Miralles, F., Lemée, R., Nézan, E., Séchet, V., 2012. Ovatoxin-a and Palytoxin Accumulation in seafood in relation to *Ostreopsis* cf. *ovata* blooms on the French Mediterranean coast. *Mar. Drugs* 10, 477–496.
- Bagnis, R., Bennett, J., Prieur, C., Legrand, A.-M., 1985. The dynamics of three toxic benthic dinoflagellates and the toxicity of ciguateric surgeonfish in French Polynesia, in: Anderson, D.M., White, A.W., Baden, D.G. (Eds.), *Toxic Dinoflagellates*. Proceedings of the Third

International Conference on Toxic Dinoflagellates. Presented at the Third International Conference on Toxic Dinoflagellates, Elsevier, New York, St. Andrews, New Brunswick, Canada, pp. 177–182.

- Ballantine, D., L., Tosteson, T.R., Bardales, A.T., 1988. Population dynamics and toxicity of natural populations of benthic dinoflagellates in southwestern Puerto Rico. *J. Exp. Mar. Biol. Ecol.* 119, 201–212.
- Beck, H.E., Zimmermann, N.E., McVicar, T.R., Vergopolan, N., Berg, A., Wood, E.F., 2018. Present and future Köppen-Geiger climate classification maps at 1-km resolution. *Sci. Data* 5, 180214. <https://doi.org/10.1038/sdata.2018.214>
- Berdalet, E., Chinain, M., Fraga, S., Lemée, R., Litaker, W., Penna, A., Usup, G., Vila, M., Zingone, A., 2017. Harmful Algal Blooms in Benthic Systems: Recent Progress and Future Research. *Oceanography* 30, 36–45. <https://doi.org/10.5670/oceanog.2017.108>
- Besada, E.G., Loeblich, L.A., Loeblich, A.R., III, 1982. Observations on tropical, benthic dinoflagellates from ciguatera-endemic areas: *Coolia*, *Gambierdiscus* and *Ostreopsis*. *Bull. Mar. Sci.* 32, 723–735.
- Brissard, C., Herrenknecht, C., Séchet, V., Hervé, F., Pisapia, F., Harcouet, J., Lemée, R., Chomérat, N., Hess, P., Amzil, Z., 2014. Complex toxin profile of French Mediterranean *Ostreopsis* cf. *ovata* strains, seafood accumulation and ovatoxins prepurification. *Mar. Drugs* 12, 2851–2876.
- Cañete, E., Diogène, J., 2008. Comparative study of the use of neuroblastoma cells (Neuro-2a) and neuroblastoma×glioma hybrid cells (NG108-15) for the toxic effect quantification of marine toxins. *Toxicon* 52, 541–550. <https://doi.org/10.1016/j.toxicon.2008.06.028>
- Carlson, R.D., Tindall, D.R., 1985. Distribution and periodicity of toxic dinoflagellates in the Virgin Islands, in: Anderson, D.M., White, A.W., Baden, D.G. (Eds.), *Toxic Dinoflagellates*. Proceedings of the Third International Conference on Toxic Dinoflagellates. Presented at the

International Conference on Toxic Dinoflagellates, Elsevier, New York, St. Andrews, New Brunswick, Canada, pp. 171–176.

- Chang, F.H., Shimizu, Y., Hay, B., Stewart, R., Mackay, G., Tasker, R., 2000. Three recently recorded *Ostreopsis* spp. (Dinophyceae) in the New Zealand: temporal and regional distribution in the upper North Island from 1995 to 1997. *N. Z. J. Mar. Freshw. Res.* 34, 29–39.
- Chinain, M., Darius, H.T., Gatti, C.M., Roué, M., 2016. Update on ciguatera research in French Polynesia. *SPC Fish. Newsl.* 150, 42–51.
- Chinain, M., Gatti, C.M., Roué, M., Darius, H.T., 2020. Ciguatera-causing dinoflagellates in the genera *Gambierdiscus* and *Fukuyoa*: Distribution, ecophysiology and toxicology, in: Subba Rao, D.V. (Ed.), *Dinoflagellates: Morphology, Life-History and Ecological Significance*. Nova Science Publishers, New-York, 66 pp.
- Chomérat, N., Couté, A., 2008. *Protoperidinium bolmonense* sp. nov. (Peridiniales, Dinophyceae), a small dinoflagellate from a brackish hypereutrophic lagoon (South of France). *Phycologia* 47, 392–403.
- Chomérat, N., Mahana iti Gatti, C., Nézan, E., Chinain, M., 2017. Studies on the benthic genus *Sinophysis* (Dinophysales, Dinophyceae) II. *S. canaliculata* from Rapa Island (French Polynesia). *Phycologia* 56, 193–203.
- Chomérat, N., Bilien, G., Derrien, A., Henry, K., Ung, A., Viallon, J., Darius, H.T., Mahana iti Gatti, C., Roué, M., Hervé, F., Réveillon, D., Amzil, Z., Chinain, M., 2019. *Ostreopsis lenticularis* Y. Fukuyo (Dinophyceae, Gonyaulacales) from French Polynesia (South Pacific Ocean): A revisit of its morphology, molecular phylogeny and toxicity. *Harmful Algae* 84, 95–111.
<https://doi.org/10.1016/j.hal.2019.02.004>
- Chomérat, N., Bilien, G., Couté, A., Quod, J.-P., 2020. Reinvestigation of *Ostreopsis mascarenensis* Quod (Dinophyceae, Gonyaulacales) from Réunion Island (SW Indian Ocean): molecular

phylogeny and emended description. *Phycologia* 1–14.

<https://doi.org/10.1080/00318884.2019.1710443>

Ciminiello, P., Dell'Aversano, C., Fattorusso, E., Forino, M., Tartaglione, L., Grillo, C., Melchiorre, N., 2008. Putative palytoxin and its new analogue, ovatoxin-a, in *Ostreopsis ovata* collected along the ligurian coasts during the 2006 toxic outbreak. *J. Am. Soc. Mass Spectrom.* 19, 111–120. <https://doi.org/10.1016/j.jasms.2007.11.001>

Ciminiello, P., Dell'Aversano, C., Iacovo, E.D., Fattorusso, E., Forino, M., Tartaglione, L., Yasumoto, T., Battocchi, C., Giacobbe, M., Amorim, A., Penna, A., 2013. Investigation of toxin profile of Mediterranean and Atlantic strains of *Ostreopsis cf. siamensis* (Dinophyceae) by liquid chromatography–high resolution mass spectrometry. *Harmful Algae* 23, 19–27. <https://doi.org/10.1016/j.hal.2012.12.002>

Ciminiello, P., Dell'Aversano, C., Iacovo, E.D., Fattorusso, E., Forino, M., Tartaglione, L., Benedettini, G., Onorari, M., Serena, F., Battocchi, C., Casabianca, S., Penna, A., 2014. First finding of *Ostreopsis cf. ovata* toxins in marine aerosols. *Environ. Sci. Technol.* 48, 3532–3540. <https://doi.org/10.1021/es405617d>

Cohu, S., Thibaut, T., Mangialajo, L., Labat, J.P., Passafiume, O., Blanfune, A., Simon, N., Cottalorda, J.M., Lemee, R., 2011. Occurrence of the toxic dinoflagellate *Ostreopsis cf. ovata* in relation with environmental factors in Monaco (NW Mediterranean). *Mar Pollut Bull* 62, 2681–91. <https://doi.org/10.1016/j.marpolbul.2011.09.022>

Darius, H.T., Roué, M., Sibat, M., Viallon, J., Gatti, C.M. iti, Vandersea, M.W., Tester, P.A., Litaker, R.W., Amzil, Z., Hess, P., Chinain, M., 2018. Toxicological investigations on the sea urchin *Tripneustes gratilla* (Toxopneustidae, Echinoid) from Anaho Bay (Nuku Hiva, French Polynesia): Evidence for the presence of Pacific ciguatoxins. *Mar. Drugs* 16, 122. <https://doi.org/10.3390/md16040122>

- Darriba, D., Taboada, G.L., Doallo, R., Posada, D., 2012. jModelTest 2: more models, new heuristics and parallel computing. *Nat. Methods* 9, 772. <https://doi.org/10.1038/nmeth.2109>
- David, H., Laza-Martínez, A., Miguel, I., Orive, E., 2013. *Ostreopsis* cf. *siamensis* and *Ostreopsis* cf. *ovata* from the Atlantic Iberian Peninsula: Morphological and phylogenetic characterization. *Harmful Algae* 30, 44–55. <https://doi.org/10.1016/j.hal.2013.08.006>
- Deeds, J.R., Schwartz, M.D., 2010. Human risk associated with palytoxin exposure. *Toxicon* 56, 150–162. <https://doi.org/10.1016/j.toxicon.2009.05.035>
- Faust, M.A., Morton, S.L., 1995. Morphology and ecology of the marine dinoflagellate *Ostreopsis labens* sp. nov. (Dinophyceae). *J. Phycol.* 31, 456–463.
- Faust, M.A., Morton, S.L., Quod, J.-P., 1996. Further SEM study of marine dinoflagellates: the genus *Ostreopsis* (Dinophyceae). *J. Phycol.* 32, 1053–1065.
- Ferreira, C.E.L., 2006. Sea urchins killed by toxic algae. *JMBA Glob. Mar Env.* 3, 23–24.
- Fukuyo, Y., 1981. Taxonomical study on benthic dinoflagellates collected in coral reefs. *Bull. Jpn. Soc. Sci. Fish.* 47, 967–978.
- Gémin, M.-P., Réveillon, D., Hervé, F., Pavaux, A.-S., Tharaud, M., Séchet, V., Bertrand, S., Lemée, R., Amzil, Z., 2020. Toxin content of *Ostreopsis* cf. *ovata* depends on bloom phases, depth and macroalgal substrate in the NW Mediterranean Sea. *Harmful Algae* 92, 101727. <https://doi.org/10.1016/j.hal.2019.101727>
- GEOHAB, 2012. Global Ecology and Oceanography of Harmful Algal Blooms, GEOHAB Core Research Project: HABs in Benthic Systems. Berdalet E., Tester P. and Zingone A. (Eds.). IOC of UNESCO and SCOR, Paris and Newark.
- Georges des Aulnois, M., Roux, P., Caruana, A., Réveillon, D., Briand, E., Hervé, F., Savar, V., Bormans, M., Amzil, Z., 2019. Physiological and metabolic responses of freshwater and brackish-water strains of *Microcystis aeruginosa* acclimated to a salinity gradient: insight

into salt tolerance. *Appl. Environ. Microbiol.* 85, e01614-19, /aem/85/21/AEM.01614-19.atom. <https://doi.org/10.1128/AEM.01614-19>

Guidi-Guilvard, L.D., Gasparini, S., Lemée, R., 2012. The Negative Impact of *Ostreopsis cf. Ovata* on Phytal Meiofauna from the Coastal NW Mediterranean. *Cryptogam. Algol.* 33, 121–128. <https://doi.org/10.7872/crya.v33.iss2.2011.121>

Guindon, S., Dufayard, J.-F., Lefort, V., Anisimova, M., Hordijk, W., Gascuel, O., 2010. New algorithms and methods to estimate Maximum-Likelihood phylogenies: assessing the performance of PhyML 3.0. *Syst. Biol.* 59, 307–21.

Holmes, M.J., Gillespie, N.C., Lewis, R.J., 1988. Toxicity and morphology of *Ostreopsis cf. siamensis* cultured from a ciguatera endemic region of Queensland, Australia, in: Choat, J.H., Barnes, D., Borowitzka, M.A., Coll, J.C., Davies, P.J., Flood, P., Hatcher, B.G., Hopley, D., Hutchings, P.A., Kinsey, D., Orme, G.R., Pichon, M., Sale, P.F., Sammarco, P., Wallace, C.C., Wilkinson, C., Wolanski, E., Bellwood, O. (Eds.), *Proceedings of the 6th International Coral Reef Symposium*, Vol. 3. Townsville, Australia, pp. 49–54.

Holmes, M.J., Lewis, R.J., Poli, M.A., Gillespie, N.C., 1991. Strain dependent production of ciguatoxin precursors (gambiertoxins) by *Gambierdiscus toxicus* (Dinophyceae) in culture. *Toxicon* 29, 761–775. [https://doi.org/10.1016/0041-0101\(91\)90068-3](https://doi.org/10.1016/0041-0101(91)90068-3)

Hoppenrath, M., Murray, S., Chomérat, N., Horiguchi, T., 2014. Marine benthic dinoflagellates - unveiling their worldwide biodiversity (Kleine Senckenberg-Reihe 54). E. Schweizerbart'sche Verlagbuchhandlung.

Ito, E., Yasumoto, T., 2009. Toxicological studies on palytoxin and ostreocin-D administered to mice by three different routes. *Toxicon* 54, 244–251. <https://doi.org/10.1016/j.toxicon.2009.04.009>

- Katoh, K., Standley, D.M., 2013. MAFFT multiple sequence alignment software version 7: improvements in performance and usability. *Mol. Biol. Evol.* 30, 772–80.
<https://doi.org/10.1093/molbev/mst010>
- Kerbrat, A.S., Amzil, Z., Pawlowicz, R., Golubic, S., Sibat, M., Darius, H.T., Chinain, M., Laurent, D., 2011. First evidence of palytoxin and 42-hydroxy-palytoxin in the marine cyanobacterium *Trichodesmium*. *Mar. Drugs* 9, 543–560.
<https://doi.org/10.3390/md9040543>
- Kumar, S., Stecher, G., Li, M., Knyaz, C., Tamura, K., 2018. MEGA X: Molecular Evolutionary Genetics Analysis across Computing Platforms. *Mol. Biol. Evol.* 35, 1547–1549.
<https://doi.org/10.1093/molbev/msy096>
- Laza-Martínez, A., Orive, E., Irati, M., 2011. Morphological and genetic characterization of benthic dinoflagellates of the genera *Coolia*, *Ostreopsis* and *Prorocentrum* from south-eastern Bay of Biscay. *Eur. J. Phycol.* 46, 45–65.
- Leaw, C.P., Lim, P.T., Asmat, A., Usup, G., 2001. Genetic Diversity of *Ostreopsis ovata* (Dinophyceae) from Malaysia. *Marine Biotechnology* 3, 246–255.
<https://doi.org/10.1007/s101260000073>
- Ledreux, A., Krys, S., Bernard, C., 2009. Suitability of the Neuro-2a cell line for the detection of palytoxin and analogues (neurotoxic phycotoxins). *Toxicon* 53, 300–308.
<https://doi.org/10.1016/j.toxicon.2008.12.005>
- Lee, B., Park, M.G., 2020. Distribution and genetic diversity of the toxic benthic dinoflagellate genus *Ostreopsis* in Korea. *Harmful Algae* 96, 101820.
<https://doi.org/10.1016/j.hal.2020.101820>
- Litaker, R.W., Vandersea, M.W., Kibler, S.R., Reece, K.S., Stokes, N.A., Lutzoni, F.M., Yonish, B.A., West, M.A., Black, M.N.D., Tester, P.A., 2007. Recognizing dinoflagellates using ITS rDNA sequences. *J. Phycol.* 43, 344–355.

- Mangialajo, L., Bertolotto, R., Cattaneo-Vietti, R., Chiantore, M., Grillo, C., Lemee, R., Melchiorre, N., Moretto, P., Povero, P., Ruggieri, N., 2008. The toxic benthic dinoflagellate *Ostreopsis ovata*: Quantification of proliferation along the coastline of Genoa, Italy. *Mar. Pollut. Bull.* 56, 1209–1214. <https://doi.org/10.1016/j.marpolbul.2008.02.028>
- Moore, R.E., Scheuer, P.J., 1971. Palytoxin: a new marine toxin from a Coelenterate. *Science* 172, 495–498.
- Nascimento, S.M., Corrêa, E.V., Menezes, M., Varela, D., Paredes, J., Morris, S., 2012. Growth and toxin profile of *Ostreopsis cf. ovata* (Dinophyta) from Rio de Janeiro, Brazil. *Harmful Algae* 13, 1–9. <https://doi.org/10.1016/j.hal.2011.09.008>
- Neves, R.A.F., Contins, M., Nascimento, S.M., 2018. Effects of the toxic benthic dinoflagellate *Ostreopsis cf. ovata* on fertilization and early development of the sea urchin *Lytechinus variegatus*. *Mar. Environ. Res.* 135, 11–17. <https://doi.org/10.1016/j.marenvres.2018.01.014>
- Nézan, E., Siano, R., Boulben, S., Six, C., Bilien, G., Chèze, K., Duval, A., Le Panse, S., Quéré, J., Chomérat, N., 2014. Genetic diversity of the harmful family Kareniaceae (Gymnodiniales, Dinophyceae) in France, with the description of *Karlodinium gentienii* sp. nov.: A new potentially toxic dinoflagellate. *Harmful Algae* 40, 75–91. <https://doi.org/10.1016/j.hal.2014.10.006>
- Norris, D.R., Bomber, J.W., Balech, E., 1985. Benthic dinoflagellates associated with ciguatera from the Florida Keys. I. *Ostreopsis heptagona* sp. nov., in: Anderson, D.M., White, A.W., Baden, D.G. (Eds.), *Toxic Dinoflagellates*. Elsevier Science publ. Co., New York, pp. 39–44.
- Onuma, Y., Satake, M., Ukena, T., Roux, J., Chanteau, S., Rasolofonirina, N., Ratsimaloto, M., Naoki, H., Yasumoto, T., 1999. Identification of putative palytoxin as the cause of clupeotoxism. *Toxicon* 37, 55–65.

- Parsons, M.L., Aligizaki, K., Dechraoui Bottein, M.-Y., Fraga, S., Morton, S.L., Penna, A., Rhodes, L., 2012. *Gambierdiscus* and *Ostreopsis*: Reassessment of the state of knowledge of their taxonomy, geography, ecophysiology, and toxicology. *Harmful Algae* 14, 107–129.
- Pavaux, A.-S., Rostan, J., Guidi-Guilvard, L., Marro, S., Ternon, E., Thomas, O.P., Lemée, R., Gasparini, S., 2019. Effects of the toxic dinoflagellate *Ostreopsis* cf. *ovata* on survival, feeding and reproduction of a phytal harpacticoid copepod. *J. Exp. Mar. Biol. Ecol.* 516, 103–113. <https://doi.org/10.1016/j.jembe.2019.05.004>
- Pawlowicz, R., Darius, H.T., Cruchet, P., Rossi, F., Caillaud, A., Laurent, D., Chinain, M., 2013. Evaluation of seafood toxicity in the Australes archipelago (French Polynesia) using the neuroblastoma cell-based assay. *Food Addit. Contam. Part A* 30, 567–586. <https://doi.org/10.1080/19440049.2012.755644>
- Peel, M.C., Finlayson, B.L., McMahon, T.A., 2007. Updated world map of the Ko'ppen-Geiger climate classification. *Hydrol Earth Syst Sci* 12.
- Pelin, M., Forino, M., Brovedani, V., Tartaglione, L., Dell'Aversano, C., Pistocchi, R., Poli, M., Sosa, S., Florio, C., Ciminiello, P., Tubaro, A., 2016. Ovatoxin-a, A Palytoxin Analogue Isolated from *Ostreopsis* cf. *ovata* Fukuyo: Cytotoxic Activity and ELISA Detection. *Environ. Sci. Technol.* 50, 1544–1551. <https://doi.org/10.1021/acs.est.5b04749>
- Penna, A., Vila, M., Fraga, S., Giacobbe, M.G., Andreoni, F., Riobó, P., Vernesi, C., 2005. Characterization of *Ostreopsis* and *Coolia* (Dinophyceae) isolates in the western mediterranean sea based on morphology, toxicity and internal transcribed spacer 5.8S rDNA sequences. *J. Phycol.* 41, 212–225.
- Quod, J.-P., 1994. *Ostreopsis mascarenensis* sp. nov. (Dinophyceae), dinoflagellé toxique associé à la ciguatera dans l'océan Indien. *Cryptogam. Algol.* 15, 243–251.
- Randall, J.E., 2005. Review of clupeotoxism, an often fatal illness from the consumption of clupeoid fishes. *Pac. Sci.* 59, 73–77. <https://doi.org/10.1353/psc.2005.0013>

- Rasband, W.S., 1997. ImageJ. National Institutes of Health, Bethesda, Maryland.
- Rhodes, L., Adamson, J., Suzuki, T., Briggs, L., Garthwaite, I., 2000. Toxic marine epiphytic dinoflagellates, *Ostreopsis siamensis* and *Coolia monotis* (Dinophyceae), in New Zealand. N. Z. J. Mar. Freshw. Res. 34, 371–383.
- Rhodes, L., 2011. World-wide occurrence of the toxic dinoflagellate genus *Ostreopsis* Schmidt. Toxicon 57, 400–407. <https://doi.org/10.1016/j.toxicon.2010.05.010>
- Rhodes, L.L., Smith, K.F., Verma, A., Murray, S., Harwood, D.T., Trnski, T., 2017. The dinoflagellate genera *Gambierdiscus* and *Ostreopsis* from subtropical Raoul Island and North Meyer Island, Kermadec Islands. N. Z. J. Mar. Freshw. Res. 51, 490–504. <https://doi.org/10.1080/00288330.2016.1270337>
- Ronquist, F., Huelsenbeck, J.P., 2003. MrBayes 3: Bayesian phylogenetic inference under mixed models. Bioinformatics 19, 1572–1574.
- Sato, S., Nishimura, T., Uehara, K., Sakanari, H., Tawong, W., Hariganeya, N., Smith, K., Rhodes, L., Yasumoto, T., Taira, Y., Suda, S., Yamaguchi, H., Adachi, M., 2011. Phylogeography of *Ostreopsis* along west Pacific coast, with special reference to a novel clade from Japan. Plos One 6, e27983. <https://doi.org/10.1371/journal.pone.0027983>
- Schiller, J., 1937. Dinoflagellatae (Peridineae), in: Rabenhorst, L. (Ed.), Kryptogamen-Flora von Deutschland, Österreich Und Der Schweiz, Teil. 2. Akademische Verlagsgesellschaft M.B.H., Leipzig, 589 pp.
- Schmidt, J., 1901. Preliminary report of the botanical results of the Danish expedition to Siam (1899-1900). Part IV, Peridiniales. Bot. Tidsskr. 24, 212–221.
- Selina, M.S., Orlova, T.Y., 2010. First occurrence of the genus *Ostreopsis* (Dinophyceae) in the Sea of Japan. Bot. Mar. 53, 243–249. <https://doi.org/10.1515/bot.2010.033>

- Shears, N.T., Ross, P.M., 2009. Blooms of benthic dinoflagellates of the genus *Ostreopsis*; an increasing and ecologically important phenomenon on temperate reefs in New Zealand and worldwide. *Harmful Algae* 8, 916–925. <https://doi.org/10.1016/j.hal.2009.05.003>
- Smith, K.F., Kohli, G.S., Murray, S.A., Rhodes, L.L., 2017. Assessment of the metabarcoding approach for community analysis of benthic-epiphytic dinoflagellates using mock communities. *N. Z. J. Mar. Freshw. Res.* 51, 555–576. <https://doi.org/10.1080/00288330.2017.1298632>
- Suzuki, T., Watanabe, R., Uchida, H., Matsushima, R., Nagai, H., Yasumoto, T., Yoshimatsu, T., Sato, S., Adachi, M., 2012. LC-MS/MS analysis of novel ovatoxin isomers in several *Ostreopsis* strains collected in Japan. *Harmful Algae* 20, 81–91. <https://doi.org/10.1016/j.hal.2012.08.002>
- Tartaglione, L., Dello Iacovo, E., Mazzeo, A., Casabianca, S., Ciminiello, P., Penna, A., Dell’Aversano, C., 2017. Variability in toxin profiles of the Mediterranean *Ostreopsis* cf. *ovata* and in structural features of the produced ovatoxins. *Environ. Sci. Technol.* 51, 13920–13928. <https://doi.org/10.1021/acs.est.7b03827>
- Tawong, W., Nishimura, T., Sakanari, H., Sato, S., Yamaguchi, H., Adachi, M., 2014. Distribution and molecular phylogeny of the dinoflagellate genus *Ostreopsis* in Thailand. *Harmful Algae* 37, 160–171. <https://doi.org/10.1016/j.hal.2014.06.003>
- Terajima, T., Uchida, H., Abe, N., Yasumoto, T., 2018a. Structure elucidation of ostreocin-A and ostreocin-E1, novel palytoxin analogs produced by the dinoflagellate *Ostreopsis siamensis*, using LC/Q-TOF MS. *Biosci. Biotechnol. Biochem.* 83, 1–10. <https://doi.org/10.1080/09168451.2018.1550356>
- Terajima, T., Uchida, H., Abe, N., Yasumoto, T., 2018b. Simple structural elucidation of ostreocin-B, a new palytoxin congener isolated from the marine dinoflagellate *Ostreopsis siamensis*, using complementary positive and negative ion liquid chromatography/quadrupole time-of-

flight mass spectrometry. *Rapid Commun. Mass Spectrom.* 32, 1001–1007.

<https://doi.org/10.1002/rcm.8130>

Tester, P.A., Litaker, R.W., Berdalet, E., 2020. Climate change and harmful benthic microalgae.

Harmful Algae 101655. <https://doi.org/10.1016/j.hal.2019.101655>

Tibiriçá, C.E.J.A., Leite, I.P., Batista, T.V.V., Fernandes, L.F., Chomérat, N., Herve, F., Hess, P.,

Mafra, L.L., 2019. *Ostreopsis* cf. *ovata* bloom in Currais, Brazil: Phylogeny, toxin profile and contamination of mussels and marine plastic litter. *Toxins* 11, 446.

<https://doi.org/10.3390/toxins11080446>

Tichadou, L., Glaizal, M., Armengaud, A., Grosseil, H., Lemée, R., Kantin, R., Lasalle, J.-L.,

Drouet, G., Rambaud, L., Malfait, P., de Haro, L., 2010. Health impact of unicellular algae of the *Ostreopsis* genus blooms in the Mediterranean Sea: experience of the French

Mediterranean coast surveillance network from 2006 to 2009. *Clin. Toxicol.* 48, 839–844.

<https://doi.org/10.3109/15563650.2010.513687>

Tognetto, L., Bellato, S., Moro, I., Andreoli, C., 1995. Occurrence of *Ostreopsis ovata*

(Dinophyceae) in the Tyrrhenian Sea during Summer 1994. *Bot. Mar.* 38.

<https://doi.org/10.1515/botm.1995.38.1-6.291>

Ukena, T., Satake, M., Usami, M., Oshima, Y., Naoki, H., Fujita, T., Kan, Y., Yasumoto, T., 2001.

Structure elucidation of Ostreocin D, a palytoxin analog isolated from the dinoflagellate *Ostreopsis siamensis*. *Biosci. Biotechnol. Biochem.* 65, 2585–2588.

<https://doi.org/10.1271/bbb.65.2585>

Ukena, T., Satake, M., Usami, M., Oshima, Y., Fujita, T., Naoki, H., Yasumoto, T., 2002. Structural

confirmation of ostreocin-D by application of negative-ion fast-atom bombardment

collision-induced dissociation tandem mass spectrometric methods. *Rapid Commun. Mass*

Spectrom. 16, 2387–2393. <https://doi.org/10.1002/rcm.867>

- Usami, M., Satake, M., Ishida, S., Inoue, A., Kan, Y., Yasumoto, T., 1995. Palytoxin analogs from the dinoflagellate *Ostreopsis siamensis*. *J. Am. Chem. Soc.* 117, 5389–5390.
- Verma, A., Hoppenrath, M., Dorantes-Aranda, J.J., Harwood, D.T., Murray, S.A., 2016a. Molecular and phylogenetic characterization of *Ostreopsis* (Dinophyceae) and the description of a new species, *Ostreopsis rhodesae* sp. nov., from a subtropical Australian lagoon. *Harmful Algae* 60, 116–130. <https://doi.org/10.1016/j.hal.2016.11.004>
- Verma, A., Hoppenrath, M., Harwood, T., Brett, S., Rhodes, L., Murray, S.A., 2016b. Molecular phylogeny, morphology and toxigenicity of *Ostreopsis* cf. *siamensis* (Dinophyceae) from temperate south-east Australia. *Phycol. Res.* 64, 146–159. <https://doi.org/10.1111/pre.12128>
- Verma, A., Hughes, D.J., Harwood, D.T., Suggett, D.J., Ralph, P.J., Murray, S.A., 2020. Functional significance of phylogeographic structure in a toxic benthic marine microbial eukaryote over a latitudinal gradient along the East Australian Current. *Ecol Evol* ece3.6358. <https://doi.org/10.1002/ece3.6358>
- Vila, M., Garcés, E., Masó, M., 2001. Potentially toxic epiphytic dinoflagellate assemblages on macroalgae in the NW Mediterranean Marine Science. *Aquat. Microb. Ecol.* 26, 51–60.
- Zhang, H., Lu, S., Li, Y., Cen, J., Wang, H., Li, Q., Nie, X., 2018. Morphology and molecular phylogeny of *Ostreopsis* cf. *ovata* and *O. lenticularis* (Dinophyceae) from Hainan Island, South China Sea: *Ostreopsis* spp. from Hainan Island. *Phycol. Res.* 66, 3–14. <https://doi.org/10.1111/pre.12192>

Table 1. Distance values (pairwise uncorrected p -distances) based on the LSU D8–D10 rDNA, LSU D1–D3 rDNA and ITS–5.8S region sequences net-between and within subclades of *Ostreopsis* sp. 6.

LSU rDNA D8 – D10			subclades			
subclades	locality	n	A	B	D	E
A	Tahiti island	14	0.000			
B	Gulf of Thailand	2	0.002	0.000		
D	Iriomote / Kohama islands, Japan	2	0.013	0.013	0.002	
E	Iriomote / Okinawa islands, Japan; Korea	5	0.013	0.012	0.018	0.001

LSU rDNA D1–D3

subclades	locality	n	A	B	C	D/E?
A	Tahiti island	6	0.001			
B	Malaysia	1	0.032	n/c		
C	Viet Nam	1	0.046	0.059	n/c	
D/E?	Aka island, Japan	3	0.094	0.105	0.118	0.023

ITS–5.8S region

subclades	locality	n	A	B	C	D	E
A	Tahiti island	6	0.002				
B	Gulf of Thailand, Malaysia	4	0.008	0.004			
C	Viet Nam	2	0.074	0.068	0.008		
D	Iriomote island (Haemida), Japan	1	0.147	0.141	0.131	n/c	
E	Iriomote (Uehara), Okinawa (Uken) islands, Japan	2	0.127	0.126	0.152	0.150	0.018

Pairwise uncorrected p distance values within subclade are shown on the diagonal
n/c: not calculated

Table 2. Estimation of the toxin content of eight strains of *Ostreopsis* sp. 6 in the absence (O^- conditions) and presence (O^+ conditions) of 200 μ M ouabain, as assessed by CBA-N2a. For each strain, data represent the mean \pm SD of three independent experiments

Strain	O^- condition			O^+ condition		
	pg PITX equiv. cell ⁻¹	SD	CV (%)	pg PITX equiv. cell ⁻¹	SD	CV (%)
PNA19-1	1.73	0.31	17.8	1.14	0.12	10.6
PNA19-2	2.18	0.09	4.2	1.36	0.08	5.8
PNA19-3	1.99	0.23	11.5	1.17	0.03	2.9
PNA19-4	1.95	0.17	8.7	1.08	0.09	8.0
PNA19-6	2.39	0.11	4.6	1.40	0.14	10.3
PNA19-7	2.48	0.22	8.7	1.31	0.08	6.0
PNA19-8	2.28	0.34	14.9	1.32	0.06	4.2
PNA19-9	2.25	0.11	4.7	1.35	0.07	5.2

Table 3. Morphological data of *O. siamensis*, *O. labens* and *Ostreopsis* sp. 6 from the tropical areas, compared with ‘*O. cf. siamensis*’ from the temperate/subtropical areas

Species	Subclade (this study)	DV length (µm)	Width (µm)	DV/W	cingulum	Po plate (µm)	Thecal pores	Ocean/Sea	Study area (latitude)	Köppen-Geiger climate category ¹	Reference
<i>O. siamensis</i>	—	90F	—	—	undulated	—	1 type: large pores (Figs 5-6)	Gulf of Thailand	(≈12°N)	Am (tropical monsoon)	Schmidt (1901)
<i>O. siamensis</i>	—	60–100F	45–90F	—	undulated	—	1 type, large	Pacific Ocean	Ryukyu islands, Japan (≈24–26°N)	Cfa (subtropical humid) to Af (tropical rainforest)	Fukuyo (1981)
<i>O. cf. siamensis</i>	—	88–115F	64–93F	0.9–1.6	—	—	1 type: large	Coral Sea	Heron and Lady Elliot islands, Hoffmans rocks Australia (≈24°S)	Cwa (subtropical humid)	Holmes et al. (1988)
‘ <i>O. lenticularis</i> ’ † (misidentified)	—	65–75F	57–63F	—	—	16	1 type: large (0.4 µm)	Caribbean Sea region; Indian Ocean ; Pacific Ocean (cf. Fukuyo 1981)	Various islands (≈17°N); Réunion Island (≈21°S);	Am (tropical monsoon, Aw (tropical savanna))	Faust et al. (1996)
<i>O. labens</i>	—	81–110F 86–98F	70–80F	—	undulated (Fig. 6)	18	1 type: large (0.3 µm)	Caribbean Sea Pacific Ocean	Belize (≈17°N) Ishigaki and Iriomote islands, Japan (≈24°N)	Am (tropical monsoon)	Faust and Morton (1995) Faust et al. (1996)
<i>Ostreopsis</i> sp. 6 (as ‘ <i>O. lenticularis</i> ’)	B	64–76C	52–65C	—	—	—	1 type	South China Sea	Pulau Redang (≈6°N)	Aw (tropical savanna)	Leaw et al. (2001)
<i>Ostreopsis</i> sp. 6	B	49.9–84.3C	35.4–66.9C	1.2–1.4	undulated	16	1 type: large (0.35–0.60 µm)	Gulf of Thailand	(≈12°N)	Am (tropical monsoon)	Tawong et al. (2014)
<i>Ostreopsis</i> sp. 6 (strain 17JJ0908)	E	43–69C	36–54	1–1.4	undulated	—	— (large pores visible on pictures)	Yellow Sea	South Korea (Jeju Island, ≈34°N)	Cfa (subtropical humid)	Lee and Park (2020)
<i>Ostreopsis</i> sp. 6	A	58.0–82.5F	45.7–61.2F	1.1–1.5	undulated	17.5	2 types: large (0.34–0.65 µm) and small (0.05–0.08 µm)	Pacific Ocean	French Polynesia, Tahiti island (≈17°S)	Aw (tropical savanna)	This study

' <i>O. siamensis</i> '†	60–85F	38–45F	—	—	—	2 types: large (0.18–0.38 µm) and small (0.08–0.1 µm)	Pacific Ocean	Northern New Zealand (≈35°S)	Cfb (warm temperate oceanic)	Chang et al. (2000)
' <i>O. siamensis</i> '†	52–68C	40–55C	—	slight undulation?	11 (from Fig. 2C)	1 type	Pacific Ocean	Northern New Zealand (≈35°S)	Cfb (warm temperate oceanic)	Rhodes et al. (2000)
<i>Ostreopsis</i> sp.	30–40C	20–30C	—	—	10	1 type: 0.1–0.2 µm	Western Mediterranean Sea	Coasts of Spain, Majorca, Corsica (≈41–42°N)	Csa (warm Mediterranean)	Vila et al. (2001)
<i>O. cf. siamensis</i>	63–90F	34–56F	—	flat, not undulated	—	1 type: 0.11–0.56 µm	Mediterranean Sea	Spain, Italy (≈37–44°N)	Csa (warm Mediterranean)	Penna et al. (2005)
<i>O. cf. siamensis</i>	50–75C	38–62C	—	straight, sometimes undulated	≈11	1 type: 0.23–0.29 µm	North Aegean Sea	(≈39–41°N)	Csa (warm Mediterranean)	Aligizaki and Nikolaidis (2006)
<i>O. cf. siamensis</i>	36–66F	24–50F	1.3–1.9	straight to slightly undulated	10 (from Fig. 17)	1 type: 0.14–0.32 µm	Sea of Japan, Russia	(≈43°N)	Dwb (humid continental)	Selina and Orlova (2010)
<i>O. cf. siamensis</i>	63–78F	36–54F	—	—	7–9	1 type: 0.15–0.31 µm	Atlantic Ocean and Mediterranean Sea	Northern Spain (≈43°N) (Minorca, ≈39°N)	Cfb (temperate oceanic) and Csa (warm Mediterranean)	Laza-Martinez et al. (2011)
<i>O. cf. siamensis</i>	51–67C	33–56C	—	—	—	1 type	Mediterranean Sea / Atlantic Ocean	(≈37°N)	Csa (warm Mediterranean)	Ciminiello et al. (2013)
<i>O. cf. siamensis</i>	50–62C	41–50C	1.10–1.32	—	—	1 type	Mediterranean Sea / Atlantic Ocean	(≈37°N)	Csa (warm Mediterranean)	Ciminiello et al. (2013)
<i>O. cf. siamensis</i>	52–74.5F	27–57F	1.1–2.1	not undulated	10–12	2 types: large (0.15–0.39 µm) and small (0.07–0.13 µm)	Atlantic Ocean	Coast of Iberian peninsula (≈37–44°N)	Csa (warm Mediterranean) to Cfb (temperate oceanic)	David et al. (2013)
<i>O. cf. siamensis</i> (strain HER24)	32.3–46.9C	23.9–37.1	1.2–1.4	—	—	—	Coral Sea	Heron Island, Australia (≈23°S)	Cwa (subtropical humid)	Verma et al. (2016a)
<i>O. cf. siamensis</i>	34–47C	24.5–42C	1.1–1.7	straight	7.2–8.4	2 types	Tasman Sea (South Pacific Ocean)	Merimbula, South-east Australia (≈37°S)	Cfb (warm temperate oceanic)	Verma et al. (2016b)

† our quotation marks, indicating putatively doubtful identifications; —: no data available; F: field specimens, C: cultured cells

¹from the data of Peel et al. (2007) and Beck et al. (2018)

Figures

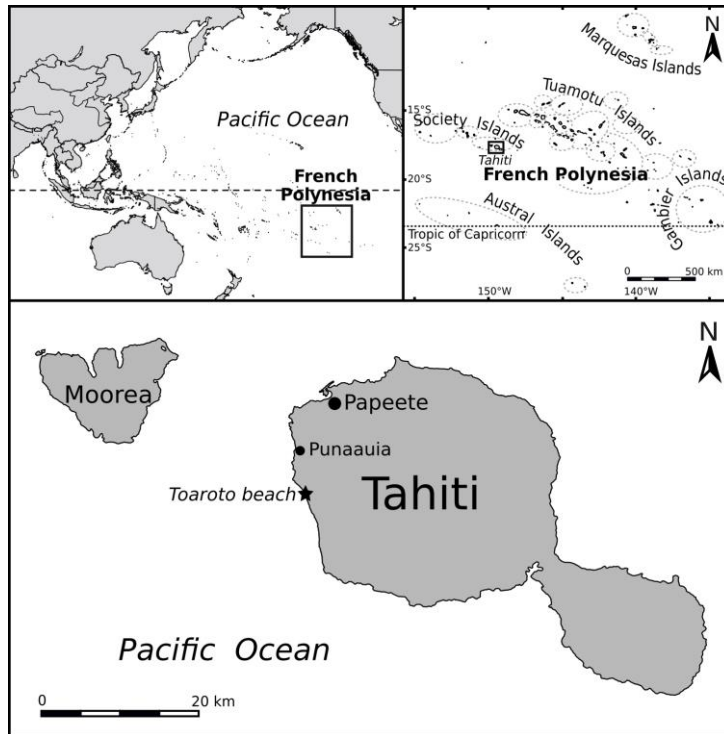


Fig. 1. Map of French Polynesia (South Pacific Ocean) and Tahiti island, showing the location of the Toaroto beach (Punaauia) where the *Ostreopsis* bloom was observed and sampled.



Fig. 2. Photographs of the benthic bloom at Toaroto beach showing the filamentous and mucilaginous brownish biofilm covering abiotic and biotic substrates including (A) macroalgae (*Turbinaria ornata* and *Dictyota bartayresiana*, (B) sponges and (C) corals (*Porites*, *Pocillopora*). (D) Light micrograph of a sample of the bloom dominated by *Ostreopsis* cells and diatoms. Scale bar: 50 μm .

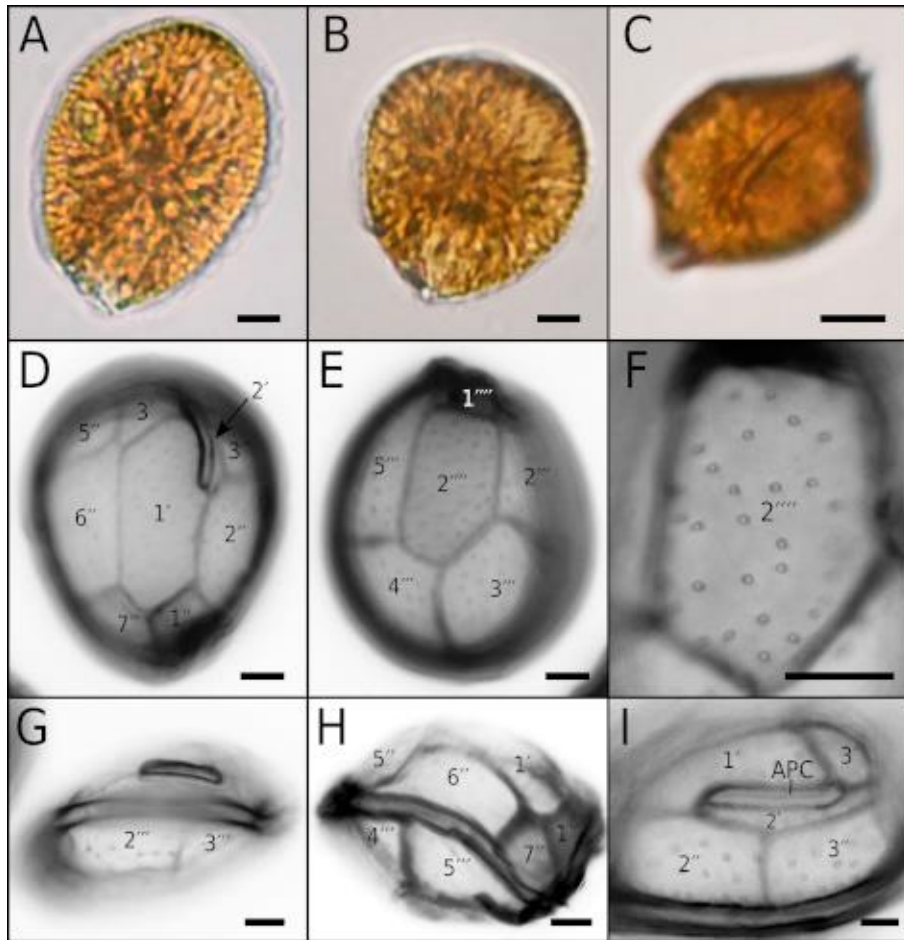


Fig. 3. Light and epifluorescence micrographs of cells from strain PNA19-9 from Toaroto beach (Punaauia, Tahiti island). (A–C) Live specimens: (A) specimen with an oval shape; (B) rounded specimen; (C) lateral view with focus on the undulated cingulum. (D–I) Epifluorescence micrographs: (D) apical view; (E) antapical view; (F) detail of the surface of 2''' plate (G) lateral view showing the undulation of the cingulum; (H) Right ventral view; (I) detail of the apical pore complex (APC) and 2' plate. Scale bars: 10 μm in A–H, 5 μm in I.

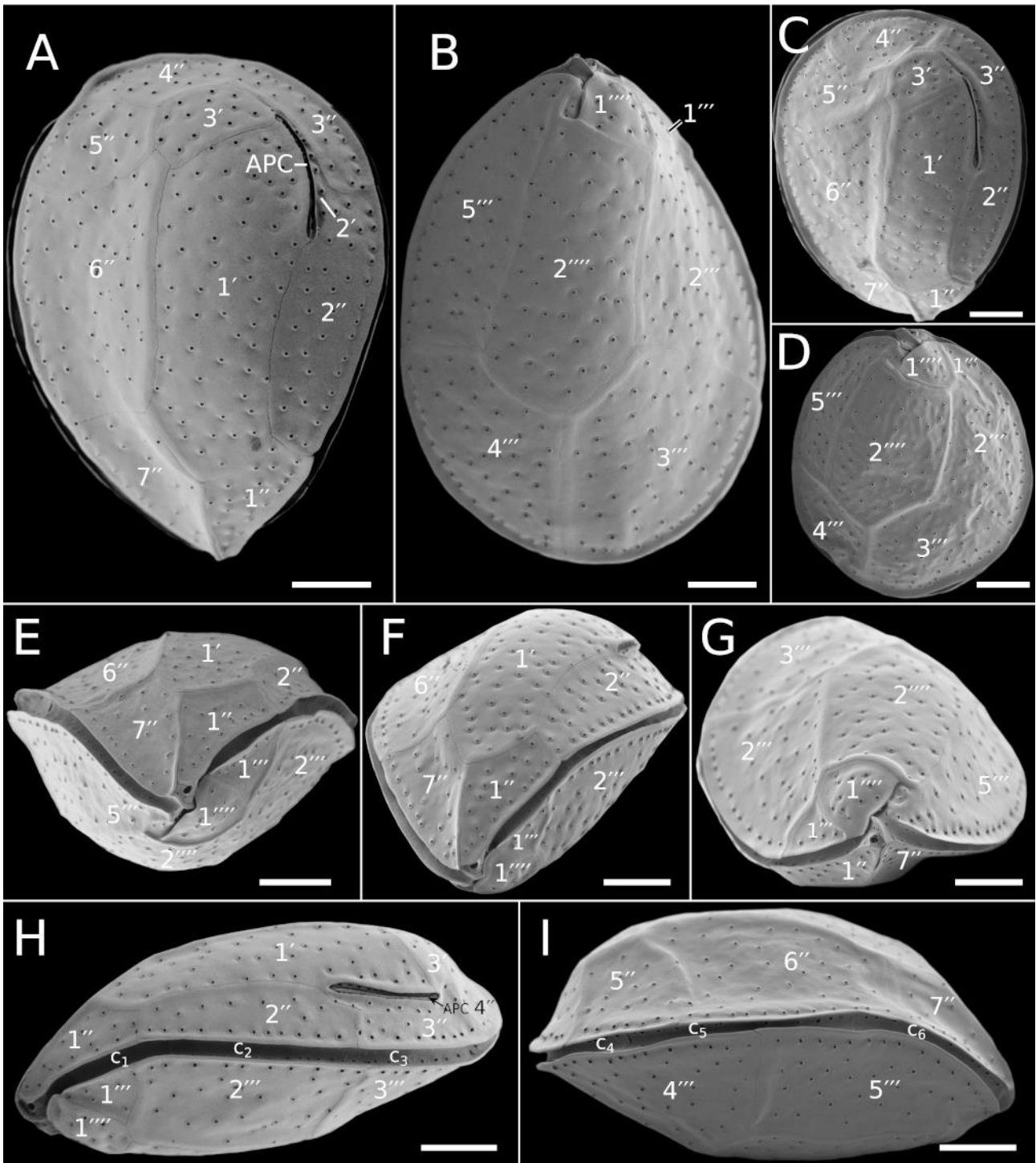


Fig. 4. Scanning electron micrographs of field specimens from the bloom of Toaroto beach (Tahiti island). (A) Apical view; (B) antapical view; (C) apical view of a smaller and less pointed specimen; (D) antapical view of a small and round specimen; (E) ventral view, note the undulated

cingulum; (F) ventro-apical view; (G) ventro-antapical view; (H) left lateral view showing the undulated cingulum and apical pore complex; (I) right lateral view. Scale bars: 10 μm .

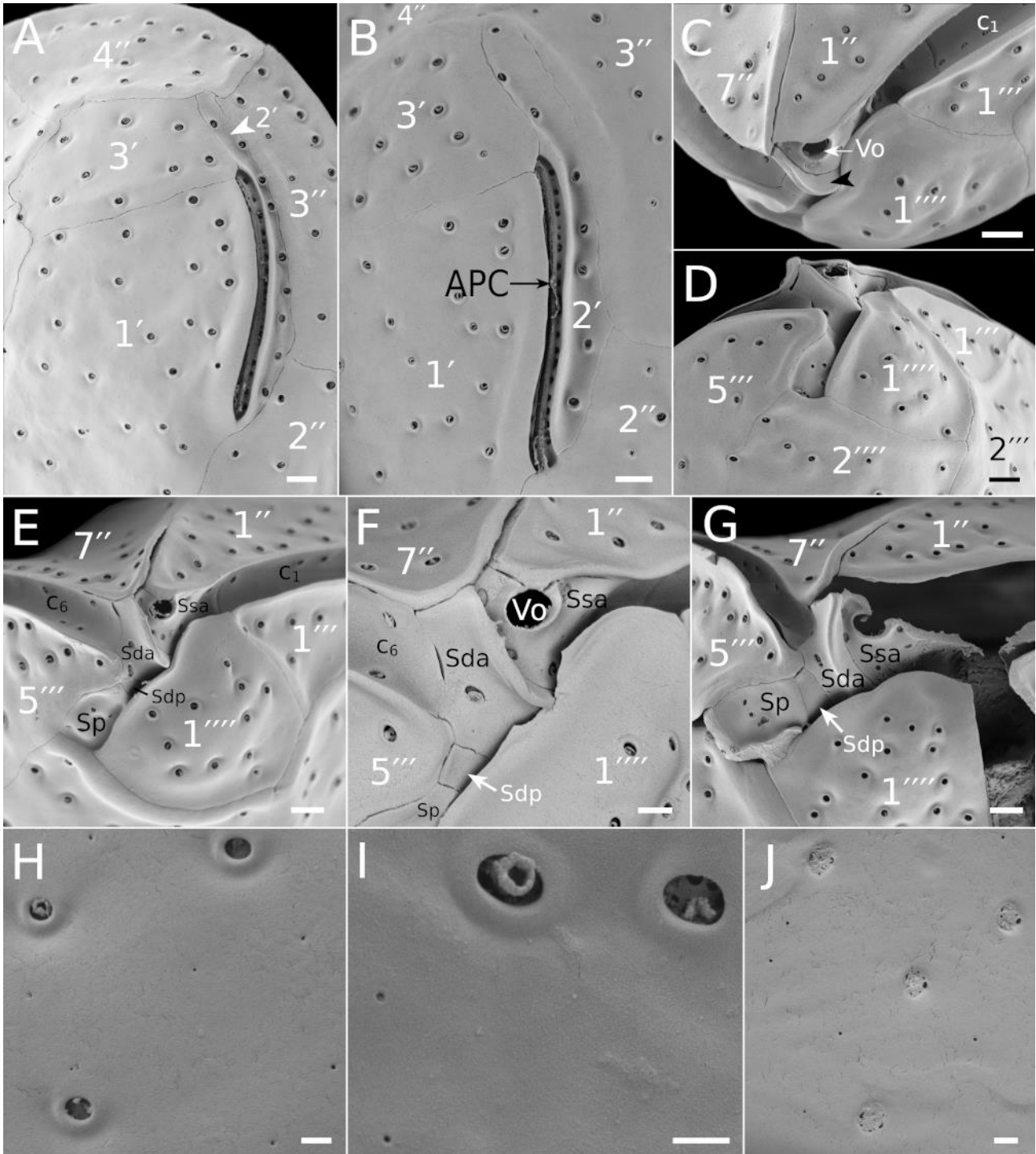


Fig. 5. Scanning electron micrographs of field specimens from the bloom of Toaroto beach (Tahiti island). (A) Detail of apical plate series and apical pore; (B) detail of the second apical (2') plate and Po plate; (C) detail of the ventral area, with the ventral opening (Vo) and list of the Sda plate (black arrowhead) visible; (D) antapical view of the sulcal area; (E) ventral view of the sulcus; (F) detail of the sulcal plates; (G) sulcal plates on a broken specimen, note the ventral opening within the Ssa plate; (H-I) Thecal pores of two sizes, note that the internal structure is visible within larger

pores; (J) internal view of thecal plates, with smaller thecal pores better visible. Scale bars: 2 μm in A, B, C, D, E and G, 1 μm in F, and 500 nm in H, I and J.

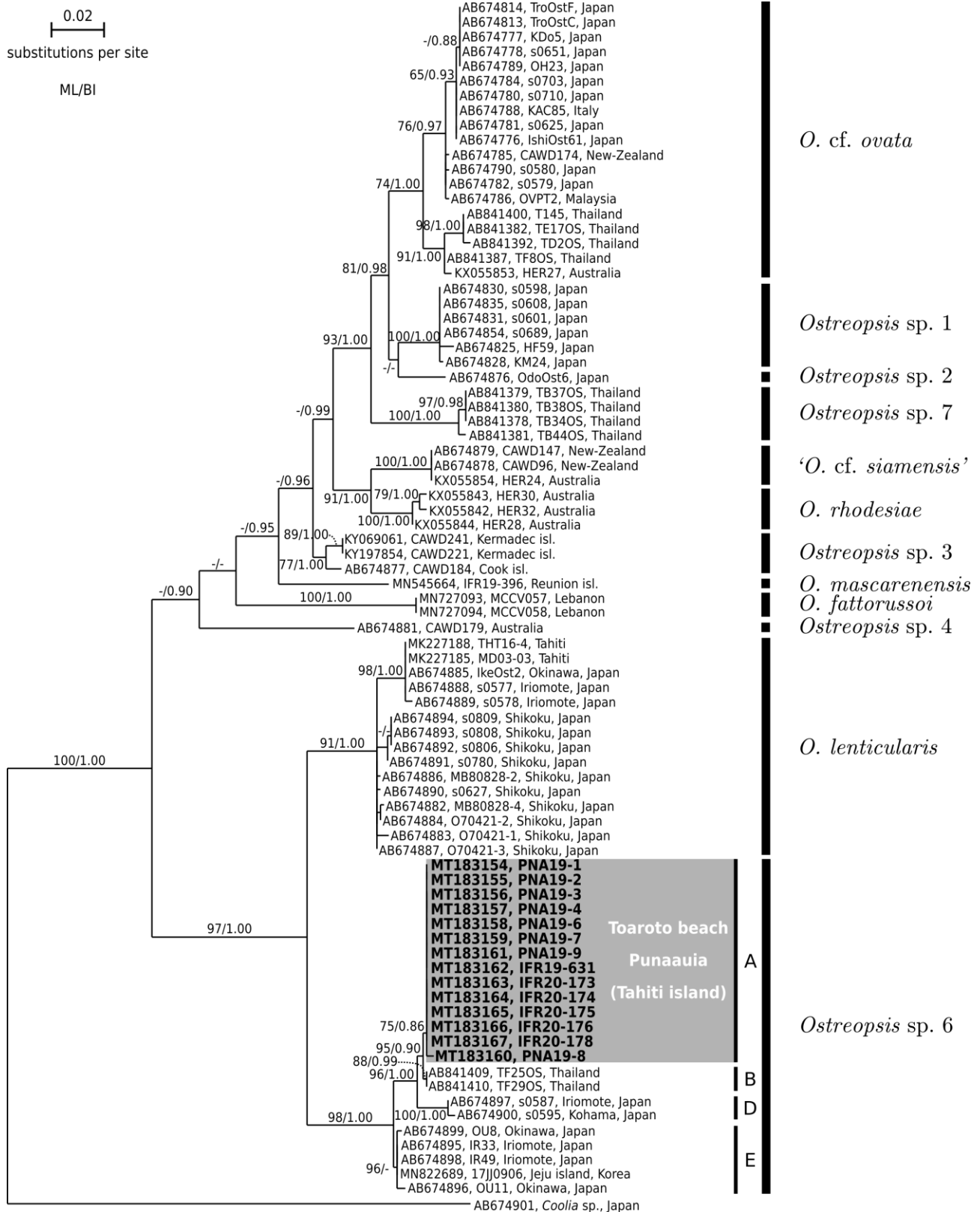


Fig. 6. Maximum Likelihood phylogenetic tree inferred from LSU rDNA D8–D10 sequences of various *Ostreopsis* strains and field specimens. Sequences from the present study are in bold face on a gray background. *Coolia* sp. is used as an outgroup. Black vertical bars show distinct *Ostreopsis*

clades. Numbers at nodes represent bootstrap support values from Maximum Likelihood (ML) and posterior probabilities from Bayesian Inference (BI). Bootstraps values below 65 and posterior probabilities below 0.70 are indicated with ‘-’.

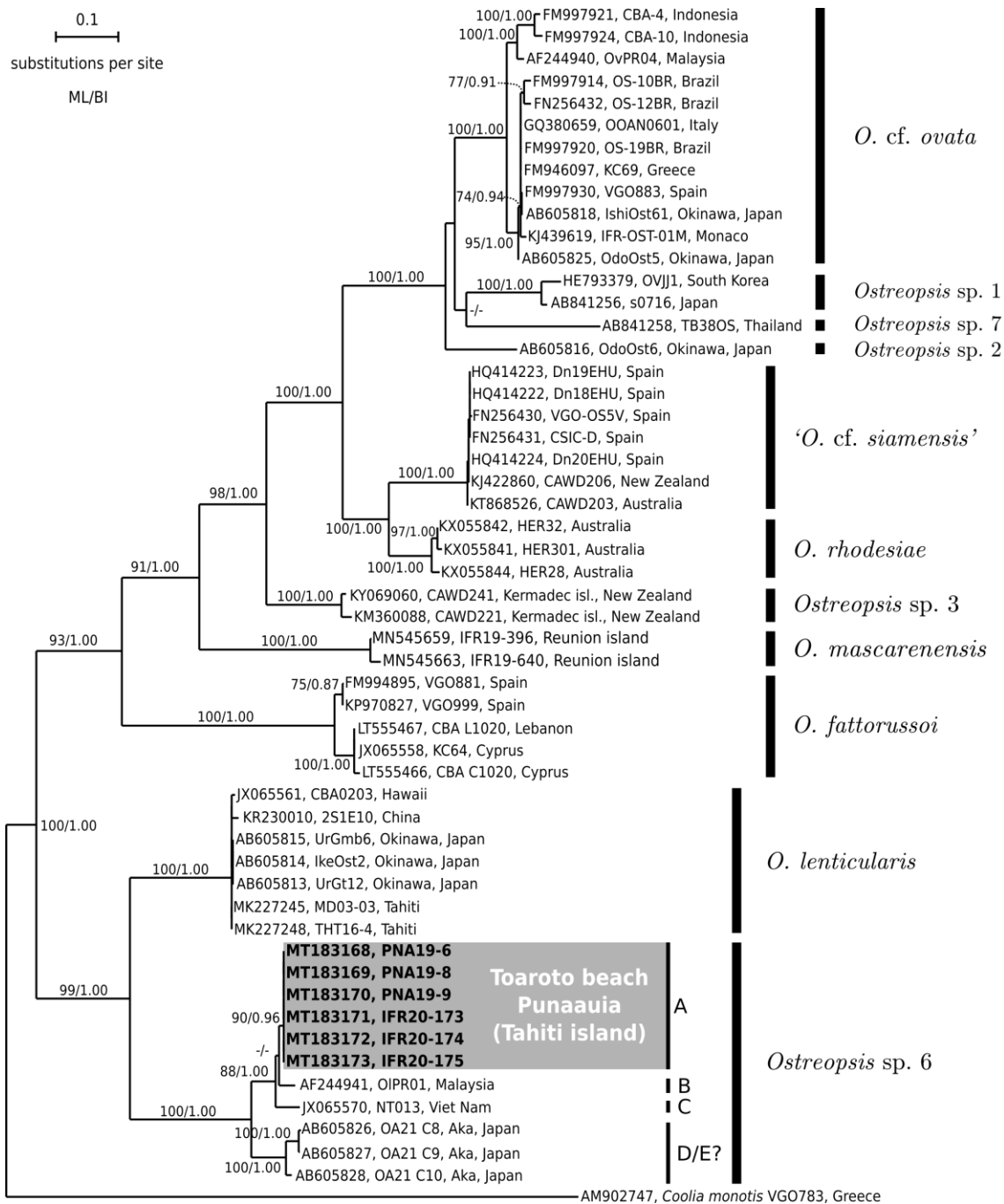


Fig. 7. Maximum Likelihood phylogenetic tree inferred from LSU rDNA D1–D3 sequences of various *Ostreopsis* strains and field specimens. Sequences from the present study are in bold face on a gray background. *Coolia monotis* is used as an outgroup. Black vertical bars show distinct *Ostreopsis* clades. Numbers at nodes represent bootstrap support values from Maximum Likelihood (ML) and posterior probabilities from Bayesian Inference (BI). Bootstraps values below 65 and posterior probabilities below 0.70 are indicated with ‘-’.

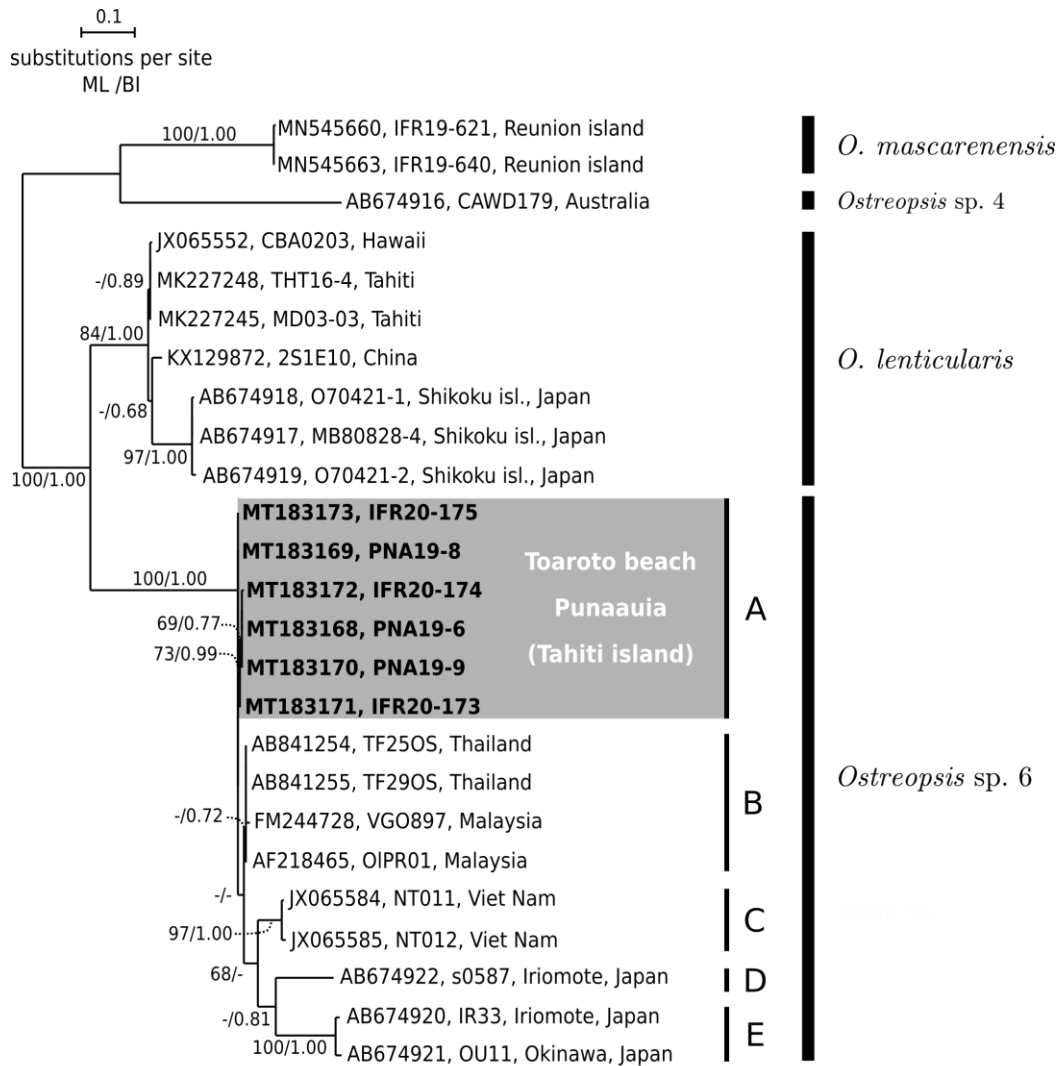


Fig. 8. Maximum Likelihood phylogenetic tree inferred from ITS–5.8S rDNA sequences of various *Ostreopsis* strains and field specimens. *Ostreopsis mascarenensis* and *Ostreopsis* sp. 4 are used as outgroup. Sequence from the present study are by bold face on a gray background. Black vertical bars show distinct *Ostreopsis* clade. Numbers at nodes represent bootstrap support values from Maximum Likelihood (ML) and posterior probabilities from Bayesian Inference (BI). Bootstraps values below 65 are indicated with ‘-’.

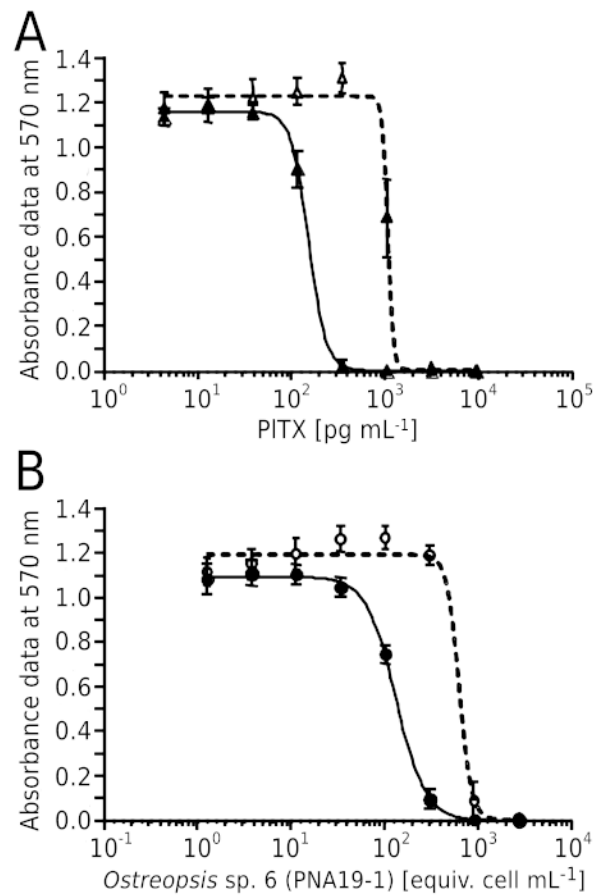


Fig. 9. Toxicity of *Ostreopsis* sp. 6 (strain PNA19-1) as assessed by means of the CBA-N2a. Dose-response curves of Neuro-2a cells when exposed to increasing concentrations of (A) standard of PITX and (B) cell extract of strain PNA19-1. Data represent the mean \pm SD of each concentration run in triplicate in three independent experiments ($n = 3$), in the absence (O^- condition, dotted lines) vs. presence of 200 μM Ouabain (O^+ conditions, plain lines). The EC_{50} values obtained in O^- and O^+ conditions were estimated at $1,074 \pm 23$ and 156 ± 17 $\mu\text{g mL}^{-1}$ for PITX, and 564 ± 19 and 137 ± 13 cell equiv. mL^{-1} for strain PNA19-1.

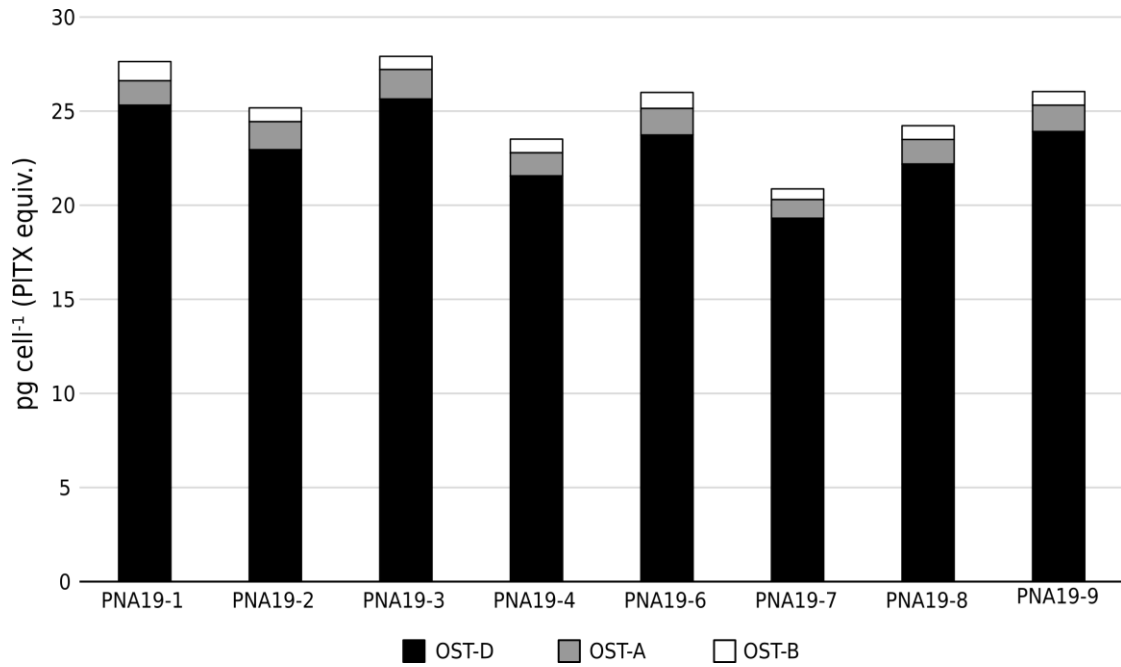


Fig. 10. Toxin contents and profiles of the eight *Ostreopsis* strains isolated from the Toaroto bloom analyzed by LC-MS/MS.

Supplementary material

Supplementary table S1. Properties of the three datasets used for phylogenetic analyses and model parameters used in maximum likelihood and bayesian inference analyses

Dataset	LSU D8–D10	LSU D1–D3	ITS–5.8S
Size (number of sequences × characters)	82 × 844	54 × 790	25 × 502
Alignment method	MAFFT q-ins-i	MAFFT q-ins-i	MAFFT q-ins-i
ML analysis (PHY-ML)			
Substitution model	TN93+I+ Γ_4	TN93+ Γ_4	HKY85+ Γ_4
Log-likelihood	-3653.66747	-7808.10852	-2378.50420
Parameters			
Gamma shape parameter	0.485	0.976	0.995
Invariant sites	0.505	0	0
Ti/Tv for purines	7.796	6.344	} 3.364370
Ti/Tv for pyrimidines	0.126	0.166	
f(A)	0.27604	0.28844	0.26738
f(C)	0.18193	0.17125	0.19639
f(G)	0.22701	0.18057	0.19373
f(T)	0.31502	0.35973	0.34249
BI analysis (MrBayes)			
Model parameters (lset)	nst=6 rates=invgamma	nst=6 rates=gamma	nst = 2 rates=gamma
Number of generations	5,000,000	5,000,000	4,000,000
Trees generated	50,001	50,001	40,001
Burnin value	15,000	10,000	12,000

Supplementary Table S2. Description of the samples analyzed for their toxicity

Sample ID	Total biomass (number of cells)	Freeze-dried sample weight (mg)	Biomass tested (equiv. cells)	Dry Extract Weight (DEW) (mg)
Field sample (bloom)	undetermined	50	undetermined	2.8
PNA19-1	1,060,745	15.1	848,596	5.8
PNA19-2	1,091,855	15	873,484	5.7
PNA19-3	1,054,712	15	843,769	5.4
PNA19-4	1,104,891	15	883,913	5.5
PNA19-6	890,122	15	712,098	6.6
PNA19-7	1,011,590	15	809,272	5.5
PNA19-8	974,924	15.1	779,940	7.0
PNA19-9	928,382	15	742,706	8.7

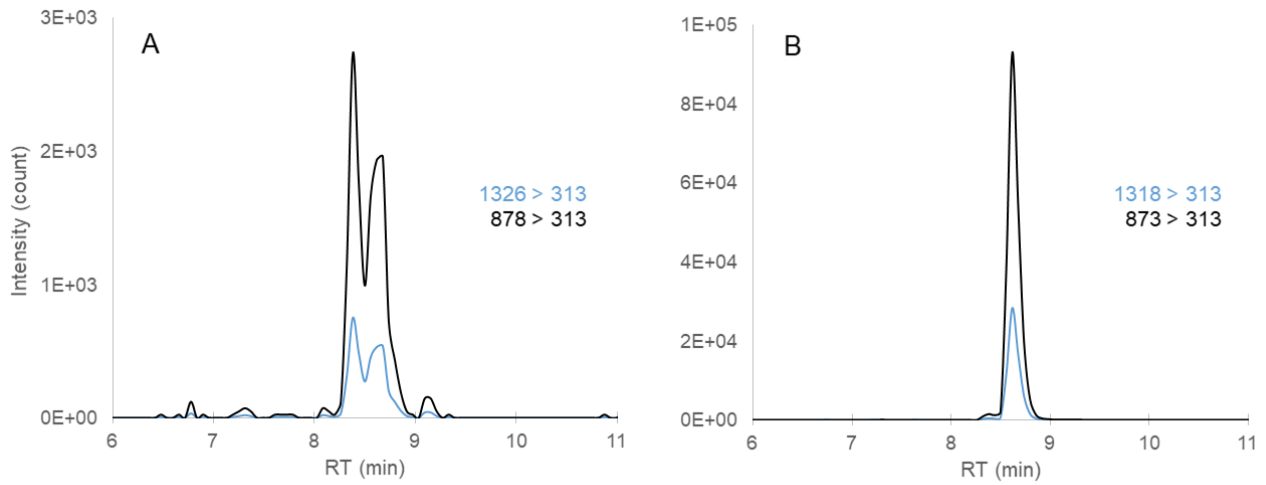


Fig. S1. LC-MS/MS chromatogram for (A) OST-A/-B and (B) OST-D (example for the strain PNA19-1). Transitions correspond to $[M+3H-H_2O]^{3+}$ (black, used for quantitation) and $[M+2H]^{2+}$ (blue) giving m/z 313.2.

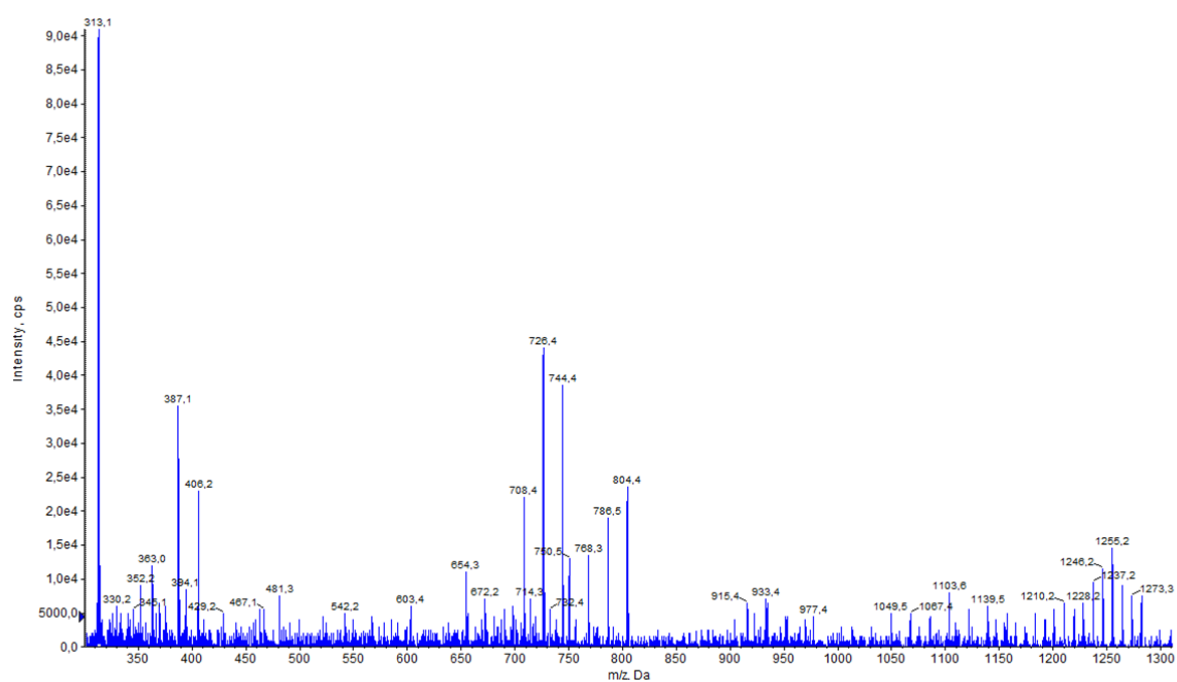
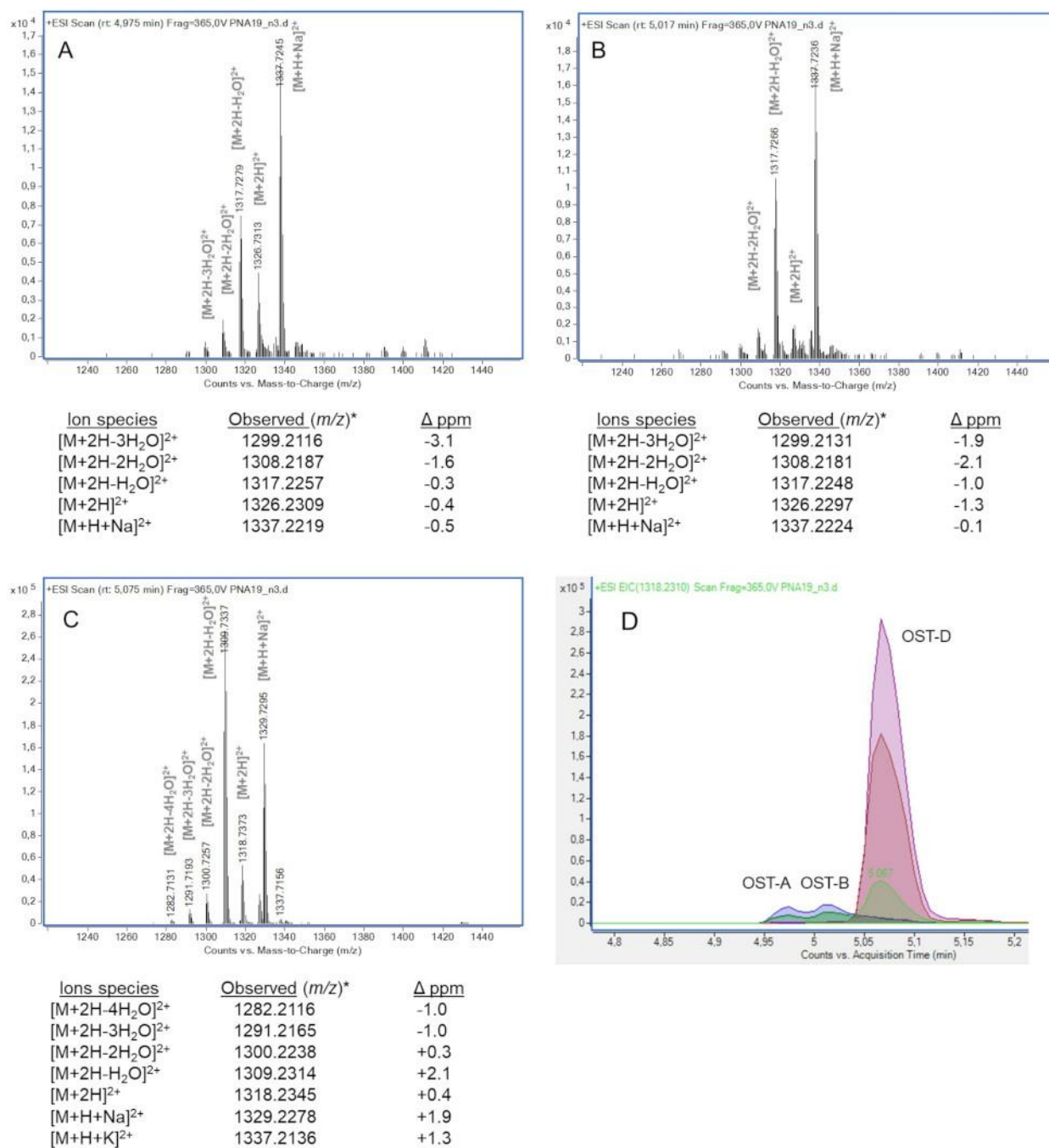


Fig. S2. Enhanced Product Ion (EPI) spectra of m/z 1309 (CE = 20 eV) showing fragments corresponding to OST-D (by comparison with fragments of mass range m/z 540–840 reported by Terajima et al. (2018a), including m/z 313.2 (specific of OSTs).



*based on the monoisotopic mass

Fig. S3. HRMS spectra (mass range m/z 1240–1440) of (A) OST-A, (B) OST-B, (C) OST-D

including assignment of doubly charged ions species and Δ ppm; (D) extracted ion chromatogram of